

High-order nonuniform time-stepping and MBP-preserving linear schemes for the time-fractional Allen–Cahn equation

Bingyin Zhang^a, Hong Wang^b, Hongfei Fu^{a,c,*}

^a*School of Mathematical Sciences, Ocean University of China, Qingdao, Shandong 266100, China*

^b*Department of Mathematics, University of South Carolina, Columbia, South Carolina 29208, USA*

^c*Laboratory of Marine Mathematics, Ocean University of China, Qingdao, Shandong 266100, China*

Abstract

In this paper, we present a class of nonuniform time-stepping, high-order linear stabilized schemes that can preserve both the discrete energy stability and maximum-bound principle (MBP) for the time-fractional Allen–Cahn equation. To this end, we develop a new prediction strategy to obtain a second-order and MBP-preserving predicted solution, which is then used to handle the nonlinear potential explicitly. Additionally, we introduce an essential nonnegative auxiliary functional that enables the design of an appropriate stabilization term to dominate the predicted nonlinear potential, and thus to preserve the discrete MBP. Combining the newly developed prediction strategy and auxiliary functional, we propose two unconditionally energy-stable linear stabilized schemes, $L1$ and $L2-1_\sigma$ schemes. We show that the $L1$ scheme unconditionally preserves the discrete MBP, whereas the $L2-1_\sigma$ scheme requires a mild time-step restriction. Furthermore, we develop an improved $L2-1_\sigma$ scheme with enhanced MBP preservation for large time steps, achieved through a novel unbalanced stabilization term that leverages the boundedness and monotonicity of the auxiliary functional. Representative numerical examples validate the accuracy, effectiveness, and physics-preserving of the proposed methods.

Keywords: time-fractional Allen–Cahn equation, high-order linear stabilized scheme, energy stability, maximum-bound principle, nonuniform time-stepping

2020 MSC: 35K58, 35R11, 65M06, 65M12, 65M50

1. Introduction

As a diffuse interface model, the classic phase-field model has been widely applied across various research areas, including material sciences [4, 6], hydrodynamics [5, 34], biology and tumor growth [10, 12, 16, 43]. More recently, there has been growing interest in nonlocal phase-field models [1, 2, 8, 15, 17, 23, 31, 42]. The presence of nonlocal operators in the phase-field equations has been shown to significantly alter the diffusive

*Corresponding author.

Email addresses: zhangbingyin@stu.ouc.edu.cn (Bingyin Zhang), hwang@math.sc.edu (Hong Wang), fhf@ouc.edu.cn (Hongfei Fu)

dynamics, see [7, 23, 42]. For example, the authors in [23] presented a fractional Allen–Cahn phase-field model to describe the transport of the fluid mixture of two immiscible fluid phases, where the fractional order parameters are employed to control the sharpness and the decay behavior of the interface. Moreover, the alternative fractional model was shown to provide more accurate description of anomalous diffusion processes than traditional integer-order model.

In this paper, we focus on the following phase-field model involving special time nonlocality, namely the time-fractional Allen–Cahn (tFAC) equation

$${}_0^C D_t^\alpha \phi = m (\varepsilon^2 \Delta \phi + f(\phi)), \quad t > 0, \mathbf{x} \in \Omega; \quad \phi(\mathbf{x}, 0) = \phi_{\text{init}}(\mathbf{x}), \quad \mathbf{x} \in \bar{\Omega}, \quad (1.1)$$

where the spatial domain is denoted by $\Omega \subset \mathbb{R}^d$ with $d \leq 3$, and the Caputo fractional-order derivative operator ${}_0^C D_t^\alpha$ of order $\alpha \in (0, 1)$ is defined as

$${}_0^C D_t^\alpha v = \int_0^t \omega_{1-\alpha}(t-s) \partial_s v(s) ds, \quad \omega_\mu(t) := \frac{t^{\mu-1}}{\Gamma(\mu)}.$$

In (1.1), $\phi(\mathbf{x}, t)$ is the unknown phase-field function, $m > 0$ is a mobility constant, $\varepsilon > 0$ is the interaction length that describes the thickness of the transition boundary between materials, and $f(\phi) = -F'(\phi)$ is a continuously differentiable nonlinear potential function.

It is well known that when $\alpha \rightarrow 1$, the tFAC equation recovers the classical Allen–Cahn equation, which satisfies the so-called *energy dissipation law*, i.e.,

$$E[\phi](t) \leq E[\phi](s), \quad \forall t > s \quad \text{with} \quad E[\phi](t) := \int_{\Omega} \left(\frac{\varepsilon^2}{2} |\nabla \phi(\mathbf{x})|^2 + F(\phi(\mathbf{x})) \right) d\mathbf{x}, \quad (1.2)$$

and the *maximum-bound principle* (MBP), i.e.,

$$\max_{\mathbf{x} \in \bar{\Omega}} |\phi_{\text{init}}(\mathbf{x})| \leq \beta \quad \implies \quad \max_{\mathbf{x} \in \bar{\Omega}} |\phi(\mathbf{x}, t)| \leq \beta, \quad \forall t > 0, \quad (1.3)$$

see [9] for details. Regarding the energy stability of the tFAC model, the authors [42] provided the first theoretical conclusion, i.e.,

$$E[\phi](t) \leq E[\phi](0), \quad \forall t > 0, \quad (1.4)$$

which differs from the classical energy dissipation law (1.2). Moreover, it was demonstrated in [11] that the double-well tFAC equation also admits the MBP (1.3).

Another key feature of the tFAC equation is that its evolution process often requires a long time to reach a steady state and typically involves multiple time scales (see [26, 27, 29]). Therefore, an adaptive time-stepping strategy [35, 46] serves as a heuristic and available approach to enhance computational efficiency without compromising accuracy. Moreover, it is well known that solutions to subdiffusion problems, including the tFAC equation, exhibit weak singularities near the initial time, although they would be smooth away from $t = 0$, see [20, 39]. The initial weak singularity may cause loss of convergence order in numerical simulations based upon a uniform temporal mesh. However, this issue can be alleviated by employing a special nonuniform temporal mesh, e.g., the graded mesh [24, 25, 39]. These two characteristics of the tFAC equation jointly motivate the development of effective and accurate *nonuniform time-stepping* numerical methods.

To achieve stable numerical simulations and avoid nonphysical solutions, it is hence necessary to develop numerical schemes that can preserve both the discrete energy stability and MBP for the tFAC model (1.1). In [42], Tang et al. presented a first-order method combining the uniform $L1$ formula [30, 40] and the stabilization technique [44], which preserves the energy stability (1.4) and MBP (1.3) in the discrete level. By discretizing the fractional derivative using backward Euler convolution quadrature, three energy-stable and MBP-preserving schemes of order $O(\tau^\alpha)$ were proposed and analyzed in [11]. To achieve high-order (more than first-order) and MBP-preserving numerical methods, the $L1$ scheme [19], the $L1_R$ scheme [27], the $L2-1_\sigma$ scheme [26, 29], and the SFTR (shifted fractional trapezoidal rule) scheme [45] were developed. However, there are basically two limitations to the above mentioned high-order numerical schemes: (i) they treat the nonlinear term either fully or partially implicit, which implies that their unique solvability is uncertain, especially for Flory–Huggins potential case, and a nonlinear iteration must be implemented at each time step; (ii) these schemes always require certain restrictions on the time-step to preserve the discrete MBP. These motivate us to develop a novel class of high-order linear schemes that are more efficient and can preserve the discrete MBP unconditionally. Owing to its ability to facilitate the design of linear and unconditionally energy-stable schemes, the scalar auxiliary variable (SAV) method [37, 38] has been widely applied to phase-field models, including the tFAC equation; see e.g., [14, 18, 21, 33, 36]. However, due to the uncertainty in the signs of the nonlinear term coefficients (typically functions with respect to the SAV), the construction of MBP-preserving SAV-type schemes are nontrivial and compelling, particularly for high-order time discretization methods or time-fractional model problems [14, 36].

An inspiring approach is the combinations of prediction-correction method and stabilization technique proposed in [13, 21, 22] for classical Allen–Cahn type equations. They first adopted a first-order scheme to provide a predicted solution with local second-order accuracy and preservation of the MBP, and then presented their second-order schemes by controlling the nonlinear term using an artificial stabilization term. Through this strategy, second-order linear schemes with conditional [13, 22] or unconditional [21] preservation of the MBP were successfully established for the classical Allen–Cahn equation. However, it should be noted that this approach is difficult to directly apply to the tFAC model (1.1), as a first-order method no longer provides sufficiently accurate predicted solutions, although this is feasible in the integer-order case. Thus, in the current work, we shall propose a general prediction strategy capable of providing satisfactory predicted solutions. We argue that it can also serve as a more efficient alternative approach for the prediction step in the numerical methods developed in [13, 21, 22].

In this paper, we aim to design a class of linear, energy-stable, and MBP-preserving high-order nonuniform time-stepping schemes for the tFAC equation (1.1), by leveraging the stabilized exponential SAV approach, namely the sESAV. To achieve this, we introduce a novel nonnegative auxiliary functional in Section 2, which serves twofold functions: (i) it ensures that the first-order approximation of the SAV does not compromise the temporal accuracy of ϕ ; and (ii) it enables the development of an effective stabilization term, allowing us to establish an MBP-preserving scheme. In combination with the newly developed prediction strategy and auxiliary functional, we first propose a linear stabilized $L1$ -sESAV nonuniform time-stepping scheme, which possesses the following remarkable advantages:

- it is unconditionally energy-stable;
- it can unconditionally preserve the discrete MBP, which seems to be the first time such a linear, MBP-preserving, and $(2 - \alpha)$ th order $L1$ scheme is established;
- it is computationally efficient, in fact, only systems of linear algebraic equations require to be solved for $n \geq 2$.

Then, a linear stabilized $L2-1_\sigma$ -sESAV scheme is also investigated and proven to be unconditionally energy-stable, but conditionally MBP-preserving. Moreover, to further improve the $L2-1_\sigma$ -sESAV scheme for large time-step computation, we present an unbalanced $L2-1_\sigma$ -sESAV scheme by introducing a novel stabilization term based on the boundedness and monotonicity of the novel auxiliary functional. To the best of our knowledge, so far no such linear second-order scheme with provable energy stability and MBP-preserving in the discrete setting has been developed.

The remainder of the paper is organized as follows. In Section 2, we first prove the MBP for the tFAC equation under either double-well or Flory–Huggins potential. Then, we propose and analyze the fully-discrete linear stabilized $L1$ type scheme, including the unique solvability, unconditional MBP-preservation and energy-stability. Numerical experiments are conducted in Section 3 to illustrate the performance of the proposed method. In Section 4, we develop two linear stabilized $L2-1_\sigma$ -ESAV schemes, incorporating two different stabilization terms: one balanced and one unbalanced, and unconditional energy-stability and conditional MBP-preservation are also discussed and tested. Some concluding remarks are finally drawn in the last section.

2. Maximum-bound principle and stabilized $L1$ scheme

For simplicity, the whole discussion below is confined to the two-dimensional square domain $\Omega = (0, L)^2$ with periodic boundary conditions. It is worth noting that the extensions to the three-dimensional case and/or homogeneous Neumann boundary conditions present no significant difficulties. In this section, we first discuss the MBP for the tFAC equation (1.1). Assume that there exists a positive constant β such that $f(\beta) = f(-\beta) = 0$ and $F(\phi)$ satisfies the monotone conditions away from $(-\beta, \beta)$, i.e.,

$$f(\phi) > 0, \quad \forall \phi \in (-\infty, -\beta) \cap \text{Dom}(f); \quad f(\phi) < 0, \quad \forall \phi \in (\beta, \infty) \cap \text{Dom}(f). \quad (2.1)$$

Two such typical potentials are widely used in the classical Allen–Cahn equation: one is the *double-well* potential

$$F(\phi) = \frac{1}{4}(1 - \phi^2)^2, \quad f(\phi) = -F'(\phi) = \phi - \phi^3, \quad (2.2)$$

where $\text{Dom}(f) = \mathbb{R}$ and $\beta = 1$, and the other is the *Flory–Huggins* potential

$$F(\phi) = \frac{\theta}{2}[(1 + \phi) \ln(1 + \phi) + (1 - \phi) \ln(1 - \phi)] - \frac{\theta_c}{2}\phi^2, \quad f(\phi) = \frac{\theta}{2} \ln \frac{1 - \phi}{1 + \phi} + \theta_c \phi, \quad (2.3)$$

with $\theta_c > \theta > 0$, where $\text{Dom}(f) = (-1, 1)$ and $\beta \approx 0.9575$ is the positive root of $f(\rho) = 0$.

Theorem 2.1. Suppose that $\phi \in C([0, T]; C^2(\bar{\Omega})) \cap C^1((0, T], C(\bar{\Omega}))$ is a solution to the model problem (1.1) with double-well or Flory–Huggins potential. If the initial value $\max_{\mathbf{x} \in \bar{\Omega}} |\phi_{init}(\mathbf{x})| \leq \beta$, there holds

$$\max_{\mathbf{x} \in \bar{\Omega}} |\phi(\mathbf{x}, t)| \leq \beta, \quad \forall t > 0. \quad (2.4)$$

Proof. The conclusion for the double-well potential can be found in [11, Theorem 2.3]. It remains to prove the MBP (2.4) for the Flory–Huggins potential (2.3). To this aim, for any $\epsilon \in (0, \frac{1-\beta}{2})$ such that $\beta + \epsilon < 1$, we define

$$t_*(\epsilon) = \max \left\{ 0 < t \leq T \mid \max_{\mathbf{x} \in \bar{\Omega}} |\phi(\mathbf{x}, t)| = \beta + \epsilon \text{ and } \max_{\mathbf{x} \in \bar{\Omega}} |\phi(\mathbf{x}, s)| < \beta + \epsilon, \forall s \in [0, t] \right\}.$$

It is clear that $t_*(\epsilon)$ is well-defined by the continuity assumption on ϕ . Without loss of generality, assume that $\phi(\mathbf{x}, t_*(\epsilon))$ achieves the maximum absolute value at $\mathbf{x}_*(\epsilon) \in \bar{\Omega}$ and $\phi(\mathbf{x}_*(\epsilon), t_*(\epsilon)) = -\beta - \epsilon$. Then, by the regularity of ϕ and discussion in [11, Lemma 2.3], we have

$${}_0^C D_t^\alpha \phi(\mathbf{x}_*(\epsilon), t_*(\epsilon)) \leq 0.$$

Moreover, due to the periodic boundary conditions, the following estimate holds by Taylor expansion

$$\Delta \phi(\mathbf{x}_*(\epsilon), t_*(\epsilon)) \geq 0.$$

Therefore, we arrive at the result

$$0 \geq {}_0^C D_t^\alpha \phi(\mathbf{x}_*(\epsilon), t_*(\epsilon)) - m\epsilon^2 \Delta \phi(\mathbf{x}_*(\epsilon), t_*(\epsilon)) = mf(\phi(\mathbf{x}_*(\epsilon), t_*(\epsilon))) > 0,$$

where we have used (2.1) in the last inequality. This leads to a contradiction, meaning that there are no points $(\mathbf{x}_*(\epsilon), t_*(\epsilon)) \in \bar{\Omega} \times (0, T]$ such that $\phi(\mathbf{x}_*(\epsilon), t_*(\epsilon)) = -\beta - \epsilon$ for any given T and ϵ . A similar conclusion holds for the upper bound of ϕ . Thus, the MBP property (2.4) is proved for the Flory–Huggins potential, as both $T > 0$ and $\epsilon \in (0, \frac{1-\beta}{2})$ are arbitrary. \square

Introduce an auxiliary variable $R(t) = E_1[\phi] := \int_{\Omega} F(\phi) d\mathbf{x}$, and define the modified energy

$$\mathcal{E}[\phi, R] := \frac{\epsilon^2}{2} \|\nabla \phi\|_{L^2}^2 + R, \quad (2.5)$$

which is equivalent to the original energy $E[\phi]$ defined in (1.2). Moreover, let $g(\phi, R) := \frac{\exp\{R\}}{\exp\{E_1[\phi]\}}$, which is always equal to 1 at the continuous level. Then, model (1.1) can be rewritten into the following equivalent system:

$${}_0^C D_t^\alpha \phi = m(\epsilon^2 \Delta \phi + V(g(\phi, R))f(\phi)), \quad R_t = -V(g(\phi, R))(f(\phi), \phi_t), \quad (2.6)$$

where $V(\cdot)$ is an auxiliary functional satisfying the following three assumptions:

- (A1). The auxiliary functional $V(\cdot) \in C^1(\mathbb{R}) \cap W^{2,\infty}(\mathbb{R})$ such that $V(1) = 1$, $V'(1) = 0$, and there exists a positive constant K_1 such that $|V'(\cdot)| \leq K_1$;
- (A2). The auxiliary functional is nonnegative and bounded by a positive constant K_2 , i.e., $0 \leq V(\cdot) \leq K_2$;

(A3). The auxiliary functional satisfies the following monotonicity, i.e., for any $z_1, z_2 \in \mathbb{R}$ satisfy $|z_1 - 1| \leq |z_2 - 1|$, we have $|V(z_1) - 1| \leq |V(z_2) - 1|$.

By [42, Corollary 2.1], it is straightforward to verify that the new SAV system (2.6) satisfies energy stability with respect to $\mathcal{E}[\phi, R]$, i.e., $\mathcal{E}[\phi, R](t) \leq \mathcal{E}[\phi, R](0)$ for $t > 0$.

2.1. Stabilized L1-ESAV scheme

Given a positive integer M , let $h = L/M$ be the spatial grid length and set $\Omega_h := \{\mathbf{x}_h = (ih, jh) \mid 0 \leq i, j \leq M\}$. Let \mathbb{V}_h be the set of all M -periodic real-valued grid functions on Ω_h , i.e.,

$$\mathbb{V}_h := \{v \mid v = \{v_{i,j}\}_{i,j=1}^M \text{ and } v \text{ is periodic}\}.$$

Notice that \mathbb{V}_h is a finite-dimensional linear space, thus any grid function in \mathbb{V}_h and any linear operator $P : \mathbb{V}_h \rightarrow \mathbb{V}_h$ can be treated as a vector in \mathbb{R}^{M^2} and a matrix in $\mathbb{R}^{M^2 \times M^2}$, respectively.

Define the following discrete inner product, and discrete L^2 and L^∞ norms

$$\langle v, w \rangle = h^2 \sum_{i,j=1}^M v_{ij} w_{ij}, \quad \|v\| = \sqrt{\langle v, v \rangle}, \quad \|v\|_\infty = \max_{1 \leq i,j \leq M} |v_{ij}|$$

for any $v, w \in \mathbb{V}_h$. Moreover, we define a maximum-norm space with the positive constant β for the underlying MBP problem, that is

$$\mathbb{V}_\beta := \{v \mid v \in \mathbb{V}_h \text{ with } \|v\|_\infty \leq \beta\}.$$

Next, we consider a central finite difference discretization for the spatial differential operators. For any $v \in \mathbb{V}_h$, the discrete Laplace operator Δ_h is defined by

$$\Delta_h v_{ij} = \frac{1}{h^2} (v_{i+1,j} + v_{i-1,j} + v_{i,j+1} + v_{i,j-1} - 4v_{ij}), \quad 1 \leq i, j \leq M, \quad (2.7)$$

and the discrete gradient operator ∇_h is defined by

$$\nabla_h v_{ij} = \left(\frac{v_{i+1,j} - v_{ij}}{h}, \frac{v_{i,j+1} - v_{ij}}{h} \right)^T, \quad 1 \leq i, j \leq M.$$

Consider (generally nonuniform) time levels $0 = t_0 < t_1 < \dots < t_N = T$ with time steps $\tau_k := t_k - t_{k-1}$ for $1 \leq k \leq N$. Denote by $r_k := \tau_k / \tau_{k-1}$ ($k \geq 2$) the adjacent time-step ratio. Let $v^k = v(t_k)$ and the temporal difference operator $\nabla_\tau v^k = v^k - v^{k-1}$ and $\mathbb{D}_\tau v^k = \nabla_\tau v^k / \tau_k$ for $k \geq 1$. The nonuniform L1 formula of the Caputo derivative is given by

$$\mathbb{D}_\tau^\alpha v^n = \sum_{k=1}^n \int_{t_{k-1}}^{t_k} \omega_{1-\alpha}(t_n - s) \nabla_\tau v^k / \tau_k \, ds = \sum_{k=1}^n A_{n-k}^{(n)} \nabla_\tau v^k, \quad (2.8)$$

where the time-dependent convolution kernels $A_{n-k}^{(n)} := \int_{t_{k-1}}^{t_k} \frac{\omega_{1-\alpha}(t_n - s)}{\tau_k} \, ds$ satisfy the following two main properties (see [24, 28]):

(P1). The discrete kernels are positive, i.e., $A_{n-k}^{(n)} > 0$ for $1 \leq k \leq n$;

(P2). The discrete kernels are monotone, i.e., $A_{n-k+1}^{(n)} < A_{n-k}^{(n)}$ for $1 \leq k \leq n$.

Now, let $\{\phi^n, R^n\}$ be the fully discrete approximations of the exact solutions $\{\phi(t_n), R(t_n)\}$ to the original continuous problem (2.6). We apply the nonuniform $L1$ formula (2.8) and central difference approximation (2.7) to derive the following stabilized $(2 - \alpha)$ th order ESAV scheme (denoted as $L1$ -sESAV):

Step 1. Let $\hat{\phi}^0 = \phi^0 := \phi_{\text{init}}$. For $n = 1$, first solve a predicted solution $\hat{\phi}^1$ from the fully-implicit difference scheme:

$$\mathbb{D}_\tau^\alpha \hat{\phi}^1 := A_0^{(1)}(\hat{\phi}^1 - \phi^0) = m(\varepsilon^2 \Delta_h \hat{\phi}^1 + f(\hat{\phi}^1)), \quad (2.9)$$

and then, find $\{\phi^1, R^1\} \in \mathbb{V}_h \times \mathbb{R}$ by

$$\mathbb{D}_\tau^\alpha \phi^1 = m(\varepsilon^2 \Delta_h \phi^1 + V(g_h(\hat{\phi}^1, R^0))f(\hat{\phi}^1) - \kappa V(g_h(\hat{\phi}^1, R^0))(\phi^1 - \hat{\phi}^1)), \quad (2.10)$$

$$\mathbb{D}_\tau R^1 = V(g_h(\hat{\phi}^1, R^0)) \langle -f(\hat{\phi}^1) + \kappa(\phi^1 - \hat{\phi}^1), \mathbb{D}_\tau \phi^1 \rangle. \quad (2.11)$$

where $\kappa \geq 0$ is a stabilizing constant, and g_h , a discrete version of g , denoted by $g_h(v, w) := \frac{\exp\{w\}}{\exp\{E_{1h}[v]\}}$ with E_{1h} the discrete counterpart of E_1 , i.e., $E_{1h}[v] := \langle F(v), 1 \rangle$.

Step 2. For $n \geq 2$, given ϕ^{n-1} and ϕ^{n-2} , first predict a MBP-preserving solution $\hat{\phi}^n$ by post-processing the standard linear extrapolation, i.e.,

$$\hat{\phi}^n = \min \left\{ \max \left\{ (1 + r_n)\phi^{n-1} - r_n\phi^{n-2}, -\beta \right\}, \beta \right\}, \quad (2.12)$$

and then, find $\{\phi^n, R^n\} \in \mathbb{V}_h \times \mathbb{R}$ such that

$$\mathbb{D}_\tau^\alpha \phi^n = m(\varepsilon^2 \Delta_h \phi^n + V(g_h(\hat{\phi}^n, R^{n-1}))f(\hat{\phi}^n) - \kappa V(g_h(\hat{\phi}^n, R^{n-1}))(\phi^n - \hat{\phi}^n)), \quad (2.13)$$

$$\mathbb{D}_\tau R^n = V(g_h(\hat{\phi}^n, R^{n-1})) \langle -f(\hat{\phi}^n) + \kappa(\phi^n - \hat{\phi}^n), \mathbb{D}_\tau \phi^n \rangle. \quad (2.14)$$

Remark 1. In the proposed $L1$ -sESAV scheme (2.9)–(2.14), the assumption (A1) on the functional $V(\cdot)$ ensures that the first-order approximation of the auxiliary variable R does not affect the temporal convergence of the phase-field function ϕ . Actually, a direct application of Taylor expansion, together with the assumption (A1), gives us

$$V(z) = 1 + \int_1^z (z - s)V''(s)ds,$$

which implies that if z is a first-order approximation to 1, then $V(z)$ will be a second-order approximation to 1. Moreover, the non-negativity and boundedness assumption (A2) allows us to develop effective stabilization term to dominate the nonlinear potential term, leading to MBP-preserving numerical methods, see Theorems 2.8 and 4.5 for details.

Remark 2. To effectively solve the nonlinear scheme (2.9) in **Step 1** for $n = 1$, we propose the following simple iteration scheme with stabilization:

$$A_0^{(1)}(\hat{\phi}_{(\mathfrak{s})}^1 - \phi^0) = m(\varepsilon^2 \Delta_h \hat{\phi}_{(\mathfrak{s})}^1 + f(\hat{\phi}_{(\mathfrak{s}-1)}^1) - \kappa(\hat{\phi}_{(\mathfrak{s})}^1 - \hat{\phi}_{(\mathfrak{s}-1)}^1)), \quad \mathfrak{s} \geq 1, \quad (2.15)$$

Algorithm 1: Implementation of the $L1$ -sESAV scheme

- 1: Given initial value $\phi^0 = \phi_{\text{init}}$ and $R^0 = R(t_0)$.
 - 2: **if** $n = 1$ **then**
 - 3: **Step 1:** Compute $\hat{\phi}^1 := \hat{\phi}_{(\mathfrak{s})}^1$ by the iteration scheme (2.15) under a given termination tolerance tol until $\|\hat{\phi}_{(\mathfrak{s})}^1 - \hat{\phi}_{(\mathfrak{s}-1)}^1\|_\infty \leq tol$.
 - 4: **Step 2:** Compute ϕ^1 by (2.10) via $\hat{\phi}^1$ and R^0 .
 - 5: **Step 3:** Compute R^1 by (2.11) via ϕ^1 , $\hat{\phi}^1$ and R^0 .
 - 6: **end if**
 - 7: **for** $n = 2$ to N **do**
 - 8: **Step 4:** Compute $\hat{\phi}^n$ by (2.12) via ϕ^{n-1} and ϕ^{n-2} .
 - 9: **Step 5:** Compute ϕ^n by (2.13) via $\hat{\phi}^n$ and R^{n-1} .
 - 10: **Step 6:** Compute R^n by (2.14) via ϕ^n , $\hat{\phi}^n$ and R^{n-1} .
 - 11: **end for**
-

where the subscript (\mathfrak{s}) denotes the iteration index, and the initial iteration value is taken as $\hat{\phi}_{(0)}^1 = \phi^0$. In the next section, we will show that this iteration scheme (2.15) unconditionally preserves the discrete MBP, and meanwhile, the solution $\hat{\phi}_{(\mathfrak{s})}^1$ converges to the unique solution $\hat{\phi}^1$ of the nonlinear scheme (2.9). The detailed implementation of the $L1$ -sESAV scheme is summarized in Algorithm 1.

In the end of this subsection, we shall discuss the linear extrapolation error $\mathcal{R}^n[v] := v(t_n) - \hat{v}(t_n)$ for $n \geq 2$ under the nonuniform temporal grids, where $\hat{v}(t_n) := (1 + r_n)v(t_{n-1}) - r_nv(t_{n-2})$. It is well known that if v is sufficiently smooth, this interpolation can achieve second-order temporal accuracy. However, for the tFAC model that exhibits an initial weak singularity, the temporal accuracy may deteriorate. The following lemma provides an estimate of $\mathcal{R}^n[v]$, see also Appendix A for detailed proof.

Lemma 2.2. *Assume that $v \in C^2(0, T]$ and satisfies $|v_{tt}(t)| \leq C(1 + t^{\iota-2})$ for any regularity parameter $0 < \iota < 1$. Then, there exists a constant C_v that depends only on v such that*

$$|\mathcal{R}^n[v]| \leq \begin{cases} C_v ((\tau_1 + \tau_2)^\iota / \iota + t_1^{\iota-2} \tau_2^2), & n = 2, \\ C_v (t_{n-2}^{\iota-2} (\tau_{n-1} + \tau_n)^2 + t_{n-1}^{\iota-2} \tau_n^2), & 3 \leq n \leq N. \end{cases} \quad (2.16)$$

Moreover, if the graded temporal grids $t_k = T(k/N)^\gamma$ with grading parameter $\gamma \geq 1$ are employed, it follows that

$$|\mathcal{R}^n[v]| \leq C_{v,\gamma} N^{-\min\{2, \gamma\iota\}}, \quad 2 \leq n \leq N, \quad (2.17)$$

where $C_{v,\gamma}$ is a constant depending only on v and γ .

Remark 3. It is well known that under the initial weak singularity assumption, the global consistency error, which is commonly used in error analysis, attained by the $L1$ and $L2-1_\sigma$ formulas achieves the order of $\min\{2 - \alpha, \gamma\iota\}$ and $\min\{2, \gamma\iota\}$ on graded temporal grids, respectively; see [24, 25] for more details. Together with the interpolation error $\mathcal{R}^n[v]$ established in Lemma 2.2, this indicates that selecting the mesh grading parameter $\gamma = (2 - \alpha)/\iota$ for the $L1$ scheme proposed in this section and $\gamma = 2/\iota$ for the $L2-1_\sigma$ scheme introduced in Section 4 is sufficient to compensate for this singularity.

2.2. MBP-preservation and unique solvability of the prediction strategy

In this subsection, we shall show that the predicted solution $\hat{\phi}^n$ yielded by **Step 1** or **Step 2** is MBP-preserving and uniquely solvable. From (2.12), it can be seen that the conclusion is clearly valid for $n \geq 2$. It remains to consider the case $n = 1$. The following two lemmas will be used later.

Lemma 2.3 ([41]). *For any $\lambda > 0$, we have $\|(\lambda I - \Delta_h)^{-1}\|_\infty \leq \lambda^{-1}$, where I represents the identity operator.*

Lemma 2.4 ([9]). *If $\kappa \geq \|f'\|_{C[-\beta, \beta]}$ holds for some positive constant κ , then we have $|f(\xi) + \kappa\xi| \leq \kappa\beta$ for any $\xi \in [-\beta, \beta]$.*

Next, we use the well-known Banach's fixed point theorem to prove that the nonlinear scheme (2.9) is uniquely solvable and preserves the discrete MBP.

Theorem 2.5. *If $\kappa \geq \|f'\|_{C[-\beta, \beta]}$, the simple iterative scheme (2.15) unconditionally preserves the MBP for $\{\hat{\phi}_{(\mathfrak{s})}^1\}$, that is,*

$$\text{if } \|\phi^0\|_\infty \leq \beta \implies \|\hat{\phi}_{(\mathfrak{s})}^1\|_\infty \leq \beta \quad \text{for } \mathfrak{s} \geq 1. \quad (2.18)$$

Furthermore, if the first level time-step τ_1 is sufficiently small such that

$$\tau_1 \leq 1/\sqrt[\alpha]{\kappa m \Gamma(2 - \alpha)}, \quad (2.19)$$

then (i) the iterative scheme (2.15) converges to the unique solution $\hat{\phi}^1$ of the nonlinear scheme (2.9) in the maximum norm such that $\|\hat{\phi}^1\|_\infty \leq \beta$, and (ii) the L1-sESAV scheme (2.9)–(2.14) is uniquely solvable.

Proof. For any $\mathfrak{s} \geq 1$, we assume that $\|\hat{\phi}_{(\mathfrak{s}-1)}^1\|_\infty \leq \beta$. Rewrite (2.15) equivalently as

$$((A_0^{(1)} + \kappa m)I - m\varepsilon^2 \Delta_h) \hat{\phi}_{(\mathfrak{s})}^1 = A_0^{(1)} \phi^0 + m(\kappa \hat{\phi}_{(\mathfrak{s}-1)}^1 + f(\hat{\phi}_{(\mathfrak{s}-1)}^1)),$$

which together with Lemmas 2.3–2.4 and $\|\phi^0\|_\infty \leq \beta$ yields

$$(A_0^{(1)} + \kappa m) \|\hat{\phi}_{(\mathfrak{s})}^1\|_\infty \leq (A_0^{(1)} + \kappa m)\beta.$$

Thus, the conclusion (2.18) is proved.

Next, we discuss the MBP-preservation and unique solvability of the nonlinear scheme (2.9). To this aim, for any grid function $v \in \mathbb{V}_\beta$, we define the mapping $\mathcal{T} := \mathbb{V}_\beta \rightarrow \mathbb{V}_\beta$ through (2.15) by $\mathcal{T}[v] = w \in \mathbb{V}_\beta$, i.e.,

$$A_0^{(1)}(w - \phi^0) = m(\varepsilon^2 \Delta_h w + f(v) - \kappa(w - v)). \quad (2.20)$$

We shall show that \mathcal{T} is a contraction mapping under the time-step restriction (2.19) in what follows. For any $v_1, v_2 \in \mathbb{V}_\beta$, let $w_1 = \mathcal{T}[v_1]$, $w_2 = \mathcal{T}[v_2]$, and define $\delta w = w_1 - w_2$. Then it follows from (2.20) that

$$((A_0^{(1)} + \kappa m)I - m\varepsilon^2 \Delta_h) \delta w = \kappa m(v_1 - v_2) + m(f(v_1) - f(v_2)).$$

Further, Lemma 2.3 and the condition $\kappa \geq \|f'\|_{C[-\beta, \beta]}$ gives us

$$(A_0^{(1)} + \kappa m) \|\delta w\|_\infty \leq 2\kappa m \|v_1 - v_2\|_\infty.$$

As a consequence, it holds that

$$\|\mathcal{T}[v_1] - \mathcal{T}[v_2]\|_\infty = \|\delta w\|_\infty \leq \ell_{\mathcal{T}} \|v_1 - v_2\|_\infty \quad \text{with } \ell_{\mathcal{T}} = \frac{2\kappa m}{A_0^{(1)} + \kappa m}. \quad (2.21)$$

Since $A_0^{(1)} = \int_{t_0}^{t_1} \frac{\omega_1 - \alpha(t_1 - s)}{\tau_1} ds = \frac{\tau_1^{-\alpha}}{\Gamma(2-\alpha)}$, we conclude that if $\tau_1 \leq \sqrt[3]{1/(\kappa m \Gamma(2-\alpha))}$, it follows that $\ell_{\mathcal{T}} < 1$, ensuring that \mathcal{T} is a contractive mapping. By Banach's fixed point theorem, the mapping \mathcal{T} admits a unique fixed point $\hat{\phi}^1 \in \mathbb{V}_\beta$. Consequently, the iterative scheme (2.15) is convergent in the maximum norm, and the fixed point $\hat{\phi}^1$ is just the unique solution of the nonlinear scheme (2.9).

For the simplicity of presentation, below we denote $V^n := V(g_h(\hat{\phi}^n, R^{n-1}))$ for $n \geq 1$. Then, equations (2.10)–(2.11) and (2.13)–(2.14) can be equivalently and uniformly rewritten as:

$$\begin{aligned} [(A_0^{(n)} + \kappa m V^n)I - m\varepsilon^2 \Delta_h] \phi^n &= A_0^{(n)} \phi^{n-1} - \sum_{k=1}^{n-1} A_{n-k}^{(n)} \nabla_\tau \phi^k \\ &\quad + mV^n (\kappa \hat{\phi}^n + f(\hat{\phi}^n)), \end{aligned} \quad (2.22)$$

$$R^n = R^{n-1} + V^n \langle -f(\hat{\phi}^n) + \kappa(\phi^n - \hat{\phi}^n), \nabla_\tau \phi^n \rangle, \quad (2.23)$$

for $n \geq 1$. It follows from $A_0^{(n)} > 0$ that $(A_0^{(n)} + \kappa m V^n)I - m\varepsilon^2 \Delta_h$ is symmetric and positive definite, and thus (2.22)–(2.23) is uniquely solvable. The proof is completed. \square

Remark 4. Note that a useful estimate (2.21) for the contraction factor $\ell_{\mathcal{T}}$ is provided in the proof of Theorem 2.5, indicating that the iteration error decreases by at least a factor of $\ell_{\mathcal{T}}$ with each iteration. Let the initial iteration error be denoted by $\|\hat{\phi}_{(0)}^1 - \hat{\phi}^1\|_\infty \leq 2\beta$. Then, for a given termination tolerance tol , a maximum number of iterations $\mathfrak{s}^* = \left\lceil \frac{\ln(tol/2\beta)}{\ln(\ell_{\mathcal{T}})} \right\rceil + 1$ is sufficient to ensure $\|\hat{\phi}_{(\mathfrak{s}^*)}^1 - \hat{\phi}^1\| \leq tol$. Moreover, a smaller stabilization constant κ leads to faster convergence of the iterative scheme in (2.15).

2.3. Discrete energy stability and MBP of the L1-sESAV scheme

Define the discrete version energy that corresponding to (2.5):

$$\mathcal{E}_h[\phi^n, R^n] := \frac{\varepsilon^2}{2} \|\nabla_h \phi^n\|^2 + R^n, \quad n \geq 0.$$

Next, we will establish the energy stability of the L1-sESAV scheme.

Lemma 2.6 ([28]). *For fixed $n \geq 1$, the convolution kernels $\{A_{n-k}^{(n)}\}$ are positive semi-definite in the sense that*

$$\sum_{k=1}^n w_k \sum_{j=1}^k A_{k-j}^{(k)} w_j \geq 0 \quad \text{for any sequence } \{w_k\}_{k=1}^n.$$

Theorem 2.7. Assume that the conditions in Theorem 2.5 hold, the L1-sESAV scheme (2.9)–(2.14) is unconditionally energy-stable in the sense that $\mathcal{E}_h[\phi^n, R^n] \leq \mathcal{E}_h[\phi^0, R^0]$ for $n \geq 1$.

Proof. Let $n = k$ in (2.13), and then taking the inner product with $\nabla_\tau \phi^k = \phi^k - \phi^{k-1}$, we have

$$\langle \mathbb{D}_\tau^\alpha \phi^k, \nabla_\tau \phi^k \rangle = m \varepsilon^2 \langle \Delta_h \phi^k, \phi^k - \phi^{k-1} \rangle - m V^k \langle -f(\hat{\phi}^k) + \kappa(\phi^k - \hat{\phi}^k), \nabla_\tau \phi^k \rangle,$$

which, together with (2.23), leads to

$$\mathcal{E}_h[\phi^k, R^k] - \mathcal{E}_h[\phi^{k-1}, R^{k-1}] \leq -\frac{\varepsilon^2}{2} \|\nabla_h(\phi^k - \phi^{k-1})\|^2 - \frac{1}{m} \langle \mathbb{D}_\tau^\alpha \phi^k, \nabla_\tau \phi^k \rangle, \quad (2.24)$$

for $k \geq 2$. Similarly, it follows from (2.10) and (2.23) that (2.24) also holds for $k = 1$.

Now, sum the above inequality (2.24) from $k = 1$ to n , we obtain from (2.8) and Lemma 2.6 that

$$\mathcal{E}_h[\phi^n, R^n] - \mathcal{E}_h[\phi^0, R^0] \leq -\frac{1}{m} \sum_{k=1}^n \langle \mathbb{D}_\tau^\alpha \phi^k, \nabla_\tau \phi^k \rangle = -\frac{1}{m} \sum_{k=1}^n \left\langle \sum_{j=1}^k A_{k-j}^{(k)} \nabla_\tau \phi^j, \nabla_\tau \phi^k \right\rangle \leq 0,$$

which completes the proof. \square

In the following theorem, we are ready to establish the discrete MBP for the proposed L1-sESAV scheme.

Theorem 2.8. Assume that the conditions in Theorem 2.5 hold, the L1-sESAV scheme (2.9)–(2.14) unconditionally preserves the MBP for $\{\phi^n\}$, that is,

$$\text{if } \|\phi^0\|_\infty \leq \beta \implies \|\phi^n\|_\infty \leq \beta, \quad \forall n \geq 1.$$

Proof. This claim will be verified by the complete mathematical induction argument. Assume that $\|\phi^k\|_\infty \leq \beta$ for $0 \leq k \leq n-1$. From (2.12) and Theorem 2.5, we know $\|\hat{\phi}^n\|_\infty \leq \beta$, which together with (2.22) and Lemmas 2.3–2.4 leads to

$$(A_0^{(n)} + \kappa m V^n) \|\phi^n\|_\infty \leq \|A_0^{(n)} \phi^{n-1} - \sum_{k=1}^{n-1} A_{n-k}^{(n)} \nabla_\tau \phi^k\|_\infty + \kappa m V^n \beta, \quad (2.25)$$

where the assumption (A2) has been used. Due to the positivity and monotonicity of the discrete kernels $\{A_{n-k}^{(n)}\}$, it holds

$$\begin{aligned} \|A_0^{(n)} \phi^{n-1} - \sum_{k=1}^{n-1} A_{n-k}^{(n)} \nabla_\tau \phi^k\|_\infty &= \left\| \sum_{k=1}^{n-1} (A_{n-k-1}^{(n)} - A_{n-k}^{(n)}) \phi^k + A_{n-1}^{(n)} \phi^0 \right\|_\infty \\ &\leq \sum_{k=1}^{n-1} (A_{n-k-1}^{(n)} - A_{n-k}^{(n)}) \|\phi^k\|_\infty + A_{n-1}^{(n)} \|\phi^0\|_\infty \\ &\leq A_0^{(n)} \beta. \end{aligned} \quad (2.26)$$

Therefore, inserting (2.26) into (2.25) yields the conclusion for $k = n$, and thereby the proof is completed. \square

3. Numerical experiments

In this section, ample numerical tests are provided to illustrate the accuracy and structure-preserving properties of the $L1$ -sESAV scheme for the tFAC model (1.1). Note that the auxiliary functional introduced in Section 2 plays a crucial role in the construction and analysis of the MBP-preserving $L1$ -sESAV scheme. In the numerical implementation, we choose the following piecewise polynomial function that satisfies the assumptions (A1)–(A3) with $K_1 = 49/24$ and $K_2 = 1$:

$$V(z) := \begin{cases} 0, & z \in (-\infty, 0], \\ -8z^3 + 7z^2, & z \in (0, 1/2), \\ 2z - z^2, & z \in [1/2, 3/2], \\ 8z^3 - 41z^2 + 68z - 36, & z \in (3/2, 2), \\ 0, & z \in [2, \infty). \end{cases} \quad (3.1)$$

In all the following tests, we always set the stabilization constant $\kappa = \|f'\|_{C[-1,1]} = 2$ for the double-well potential (2.2), and $\kappa = \|f'\|_{C[-\beta,\beta]} \approx 8.02$ for the Flory–Huggins potential (2.3).

Moreover, to address the initial weak singularity, we adopt two types of mixed nonuniform temporal meshes composed of a graded mesh in the initial subinterval. Specifically, for given \hat{T} and \hat{N} , we split the time interval $[0, T]$ into two parts $[0, \hat{T}]$ and $[\hat{T}, T]$ with total N subintervals, and employ the graded mesh to subdivide $[0, \hat{T}]$ as follows

$$t_k = \hat{T}(k/\hat{N})^\gamma \quad \text{and} \quad \tau_k = t_k - t_{k-1}, \quad 1 \leq k \leq \hat{N}, \quad (3.2)$$

where $\gamma \geq 1$ is the mesh grading parameter. For the remainder interval $[\hat{T}, T]$, the following two different types of temporal grids are considered

- uniform mesh:

$$\tau_k = \frac{T - \hat{T}}{N - \hat{N}}, \quad \hat{N} + 1 \leq k \leq N; \quad (3.3)$$

- adaptive mesh based on the energy variation [27, 35]:

$$\tau_k = \max \left\{ \tau_{\min}, \frac{\tau_{\max}}{\sqrt{1 + \eta |\partial_\tau E^{k-1}|^2}} \right\}, \quad (3.4)$$

where τ_{\max}, τ_{\min} are predetermined maximum and minimum time steps, and η is a tunable parameter.

In the numerical tests, the maximum-norm error is measured in the sense that $e(N) := \max_{1 \leq n \leq N} \|\phi(t_n) - \phi^n\|_\infty$.

3.1. Temporal convergence

Consider the exterior-forced tFAC model

$${}_0^C D_t^\alpha \phi = m(\varepsilon^2 \Delta \phi + f(\phi)) + g(\mathbf{x}, t), \quad (\mathbf{x}, t) \in (0, 2\pi)^2 \times (0, 0.5], \quad (3.5)$$

Table 1: Time accuracy of the $L1$ -sESAV scheme with $\alpha = 0.4$ and $\iota = 0.4$

potential	N	$\gamma = 2$		$\gamma = 3$		$\gamma = 4 (= (2 - \alpha)/\iota)$	
		$e(N)$	Order	$e(N)$	Order	$e(N)$	Order
double-well	20	5.06×10^{-2}	—	1.68×10^{-2}	—	1.25×10^{-2}	—
	40	2.91×10^{-2}	0.80	7.64×10^{-3}	1.13	4.35×10^{-3}	1.52
	80	1.67×10^{-2}	0.80	3.40×10^{-3}	1.17	1.50×10^{-3}	1.54
	160	9.59×10^{-3}	0.80	1.48×10^{-3}	1.20	5.07×10^{-4}	1.56
	320	5.51×10^{-3}	0.80	6.49×10^{-4}	1.19	1.70×10^{-4}	1.57
Flory–Huggins	20	5.06×10^{-2}	—	1.61×10^{-2}	—	1.23×10^{-2}	—
	40	2.91×10^{-2}	0.80	7.50×10^{-3}	1.10	4.12×10^{-3}	1.58
	80	1.67×10^{-2}	0.80	3.37×10^{-3}	1.15	1.43×10^{-3}	1.52
	160	9.59×10^{-3}	0.80	1.48×10^{-3}	1.19	4.91×10^{-4}	1.54
	320	5.51×10^{-3}	0.80	6.48×10^{-4}	1.19	1.67×10^{-4}	1.56
$\min\{2 - \alpha, \gamma\iota\}$			0.80		1.20		1.60

with parameters $m = 0.01$ and $\varepsilon = 1$. Here, the linear part $g(\mathbf{x}, t)$ and parameter $\iota \in (0, 1)$ are chosen such that the exact solution is given by $\phi(\mathbf{x}, t) = \omega_{1+\iota}(t) \sin(x) \sin(y)$, which exhibits an initial weak singularity.

For a given mesh grading parameter $\gamma \geq 1$, we set $\hat{T} = \min\{1/\gamma, T\}$ and $\hat{N} = \lceil \frac{1}{T+1+\gamma^{-1}} \rceil$ in (3.2). The uniform temporal mesh (3.3) is employed in the remainder interval $[\hat{T}, T]$. The spatial domain is partitioned into $M = 400$ uniform elements along each spatial direction. We test the proposed $L1$ -sESAV scheme for solving (3.5) with different nonlinear potentials and a fixed regularity parameter $\iota = 0.4$. For fractional orders $\alpha = 0.4$ and 0.8 , different mesh grading parameters $\gamma = 2, 3, 4$ are considered, respectively. The corresponding numerical results are presented in Tables 1–2, from which we can observe that the expected temporal accuracy $\mathcal{O}(N^{-\min\{2-\alpha, \gamma\iota\}})$ is achieved.

Table 2: Time accuracy of the $L1$ -sESAV scheme with $\alpha = 0.8$ and $\iota = 0.4$

potential	N	$\gamma = 2$		$\gamma = 3 (= (2 - \alpha)/\iota)$		$\gamma = 4$	
		$e(N)$	Order	$e(N)$	Order	$e(N)$	Order
double-well	20	1.38×10^{-1}	—	1.00×10^{-1}	—	1.05×10^{-1}	—
	40	7.91×10^{-2}	0.80	4.59×10^{-2}	1.13	4.72×10^{-2}	1.15
	80	4.55×10^{-2}	0.80	2.09×10^{-2}	1.14	2.09×10^{-2}	1.18
	160	2.61×10^{-2}	0.80	9.28×10^{-3}	1.17	9.15×10^{-3}	1.19
	320	1.50×10^{-2}	0.80	4.11×10^{-3}	1.18	3.99×10^{-3}	1.20
Flory–Huggins	20	1.37×10^{-1}	—	1.00×10^{-1}	—	1.04×10^{-1}	—
	40	7.91×10^{-2}	0.80	4.58×10^{-2}	1.13	4.71×10^{-2}	1.15
	80	4.55×10^{-2}	0.80	2.08×10^{-2}	1.14	2.08×10^{-2}	1.18
	160	2.61×10^{-2}	0.80	9.27×10^{-3}	1.17	9.14×10^{-3}	1.19
	320	1.50×10^{-2}	0.80	4.11×10^{-3}	1.17	3.99×10^{-3}	1.20
$\min\{2 - \alpha, \gamma\iota\}$			0.80		1.20		1.20

3.2. Unconditional preservation of MBP and energy stability

In this subsection, we numerically verify the MBP and energy stability of the proposed $L1$ -sESAV scheme by simulating the spinodal decomposition of a homogeneous mixture

into two coexisting phases governed by the tFAC model (1.1) with $\alpha = 0.5$, $m = 1$, $\varepsilon = 0.01$ in $\Omega = (0,1)^2$. For the forthcoming simulations, we adopt $M = 128$, and the initial phase field is generated using uniformly distributed random data in the range $[-0.8, 0.8]$, which is highly oscillating, see Figure 1.

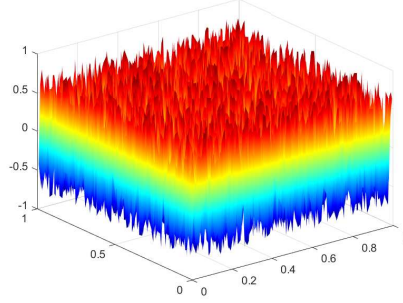


Figure 1: The initial highly-oscillated phase field

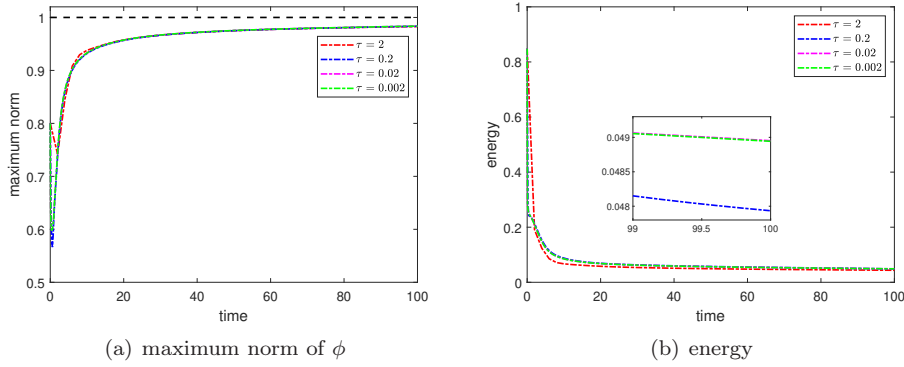


Figure 2: Time evolutions of the maximum norm and energy of simulated solutions computed by the $L1$ -sESAV scheme with different time steps: the double-well potential

Although a modified energy is introduced as an approximation of the original one to facilitate the proof of energy stability, we primarily focus on the behavior of the original (discrete) energy, which reflects the real physical mechanism of the dynamic process. In Figure 2, we show the time evolutions of the maximum norms and original energies of the numerical solutions computed using the proposed $L1$ -sESAV scheme with various time steps $\tau = 2, 0.2, 0.02, 0.002$ for the case of double-well potential. It shows that the $L1$ -sESAV scheme perfectly preserves both the MBP and the energy stability, even for large time steps (e.g., $\tau = 2$ and 0.2), which indicates the unconditional preservation of the discrete energy stability and MBP as proved Theorems 2.7–2.8. Next, we also consider the simulation of Flory–Huggins potential case and corresponding numerical results are displayed in Figure 3. Similar conclusions can also be observed.

3.3. Application of adaptive time-stepping strategy

It is well known that the dynamics process governed by the tFAC model involves multiple time scales, and typically requires a long time to reach the steady state. Hence,

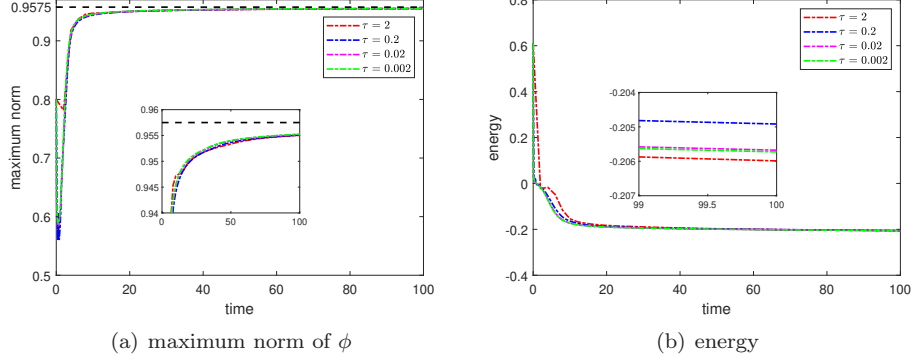


Figure 3: Time evolutions of the maximum norm and energy of simulated solutions computed by the $L1$ -sESAV scheme with different time steps: the Flory-Huggins potential

an adaptive time-stepping strategy (e.g., (3.4)) is an effective means for improving the computational efficiency without sacrificing accuracy. In our computations, the graded mesh with $\hat{T} = 0.5$, $\hat{N} = 30$ and $\gamma = (2 - \alpha)/\alpha$ is employed in the initial interval $[0, \hat{T}]$, and the remainder $[\hat{T}, T]$ is partitioned using three different types of temporal meshes, i.e., uniform large time step $\tau = 2$ and small time step $\tau = 0.02$, and adaptive time step based on (3.4), with the parameters $\tau_{\max} = 2, \tau_{\min} = 0.02, \eta = 10^6$. The other settings are the same as those used in subsection 3.2.

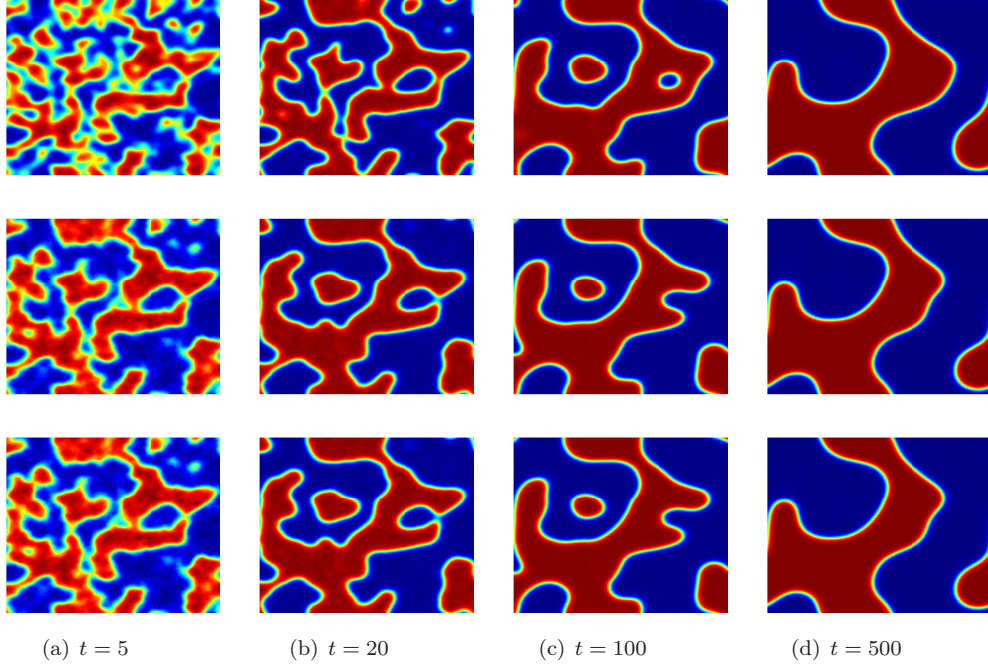


Figure 4: The dynamic snapshots of the numerical solution ϕ obtained by the $L1$ -sESAV scheme with the uniform (top, $\tau = 2$; bottom, $\tau = 0.02$) and adaptive (middle) time steps: the double-well potential

Figure 4 presents a comparison of the solution snapshots obtained using the three types of temporal meshes up to $T = 500$ for the double-well potential case. It is observed that the usage of large time step $\tau = 2$ yields an inaccurate ϕ , whereas the adaptive time-stepping strategy provides consistent coarsening patterns with those obtained using the uniform small time step $\tau = 0.02$. Besides, the evolutions of the maximum-norm of ϕ and the energy over time are depicted in Figures 5(a)–5(b), from which we can observe that (i) the proposed $L1$ -sESAV scheme is energy-stable and MBP-preserving; (ii) the time evolution curves of the maximum-norm of ϕ and energy obtained by the adaptive strategy matches very well with those generated by the uniform small time step. Moreover, Table 3 indicates the high efficiency of the proposed scheme combined with the adaptive strategy (3.4). For instance, it takes more than one and a half hours for the implementation of the small time step case, whereas the adaptive method requires only about 12 seconds! In fact, the total number of adaptive time steps is only 577, which is significantly fewer than in the uniform small time step case. This improvement is mainly due to the frequent use of large time steps in the adaptive method, as shown in Figure 5(c), only a few small time steps are employed when the energy decays rapidly. For the Flory–Huggins potential, similar conclusions can also be drawn from Figures 6–7 and Table 3.

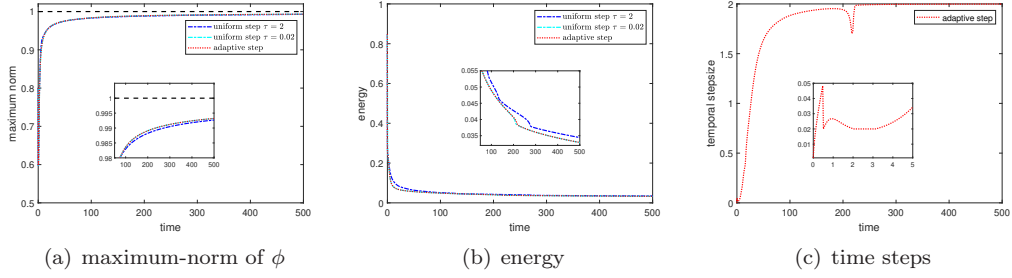


Figure 5: Time evolutions of the maximum norm (left), energy (middle), and time steps (right) for the $L1$ -sESAV scheme: the double-well potential

Table 3: CPU times and the total number of time steps yielded by the $L1$ -sESAV scheme

time-stepping strategy	double-well potential		Flory–Huggins potential	
	N	CPU times	N	CPU times
uniform step $\tau = 2$	281	4.81 s	281	4.82 s
adaptive step	577	11.17 s	598	12.05 s
uniform step $\tau = 0.02$	25007	1 h 39 m 24 s	25007	1 h 40 m 24 s

3.4. Dynamical behaviour governed by the $tFAC$ model

In order to discover the influence of fractional order α on the dynamical behaviour, we consider the $tFAC$ model (1.1) with $m = 1$, $\varepsilon = 0.01$, and double-well potential. The initial state is chosen as $\phi_{\text{init}}(x, y) = \tanh \frac{1.5 + 1.2 \cos(6\vartheta) - 2\pi r}{\sqrt{2}\lambda}$ with $\vartheta = \arctan \frac{y-0.5}{x-0.5}$ and $r = \sqrt{(x-0.5)^2 + (y-0.5)^2}$. The computational domain $\Omega = (0, 1)^2$ is divided uniformly into 128 parts in each direction.

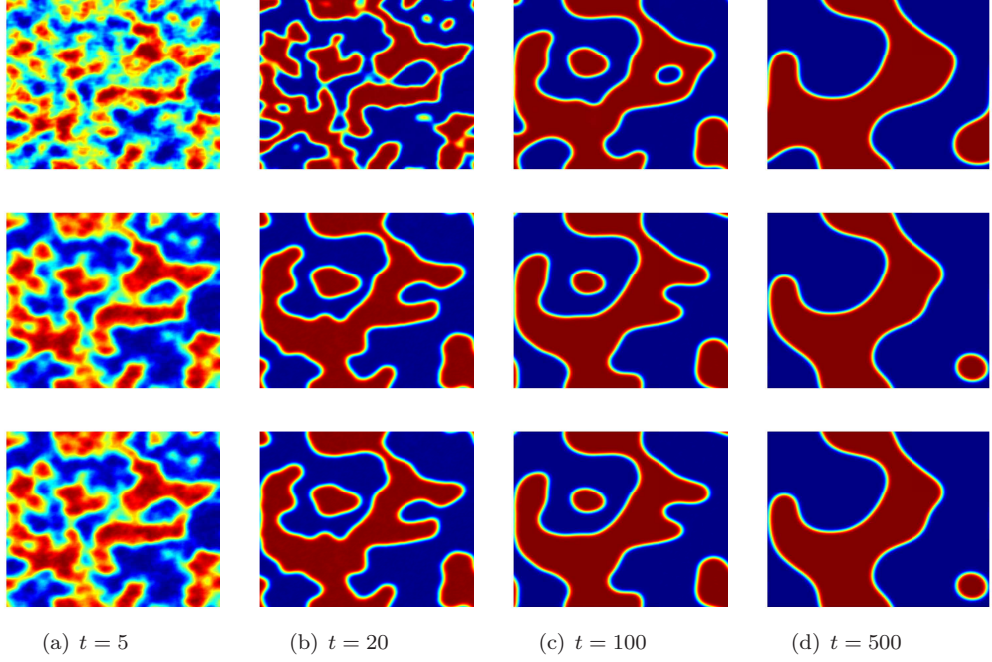


Figure 6: The dynamic snapshots of the numerical solution ϕ obtained by the $L1$ -sESAV scheme with the uniform (top, $\tau = 2$; bottom, $\tau = 0.02$) and adaptive (middle) time steps: the Flory–Huggins potential

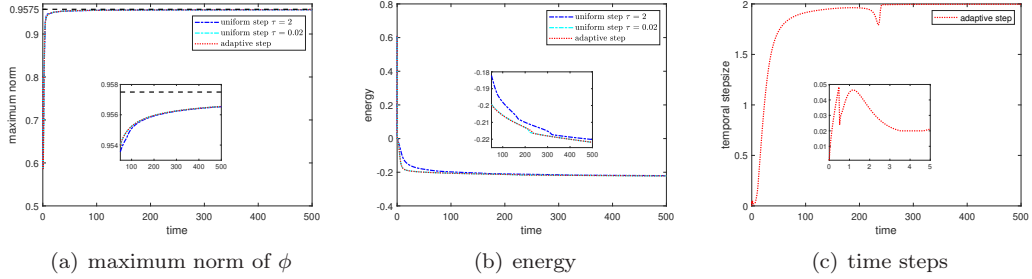


Figure 7: Time evolutions of the maximum norm (left), energy (middle), and time steps (right) for the $L1$ -sESAV scheme: the Flory–Huggins potential

In the adaptive time-stepping strategy (3.4), we set $\tau_{\max} = 2$, $\tau_{\min} = 0.02$, and the parameter $\eta = 10^7$. The time evolutions of the phase-field function with different fractional orders $\alpha = 0.9, 0.7$ and 0.4 at different time instants are shown in Figure 8. It is clearly seen that the dynamical behaviour is significantly affected by the fractional order: the bigger the α is, the faster the dynamics evolves. Thus, smaller value of α requires a longer time to reach equilibrium. This observation is further confirmed by the energy curves shown in Figure 9. In fact, for $\alpha = 0.9$, the dynamical process reaches the steady state around $t = 600$ and the corresponding energy is nearly zero; while for $\alpha = 0.7$ and 0.4 , even at $t = 700$, it has not reached the steady state.

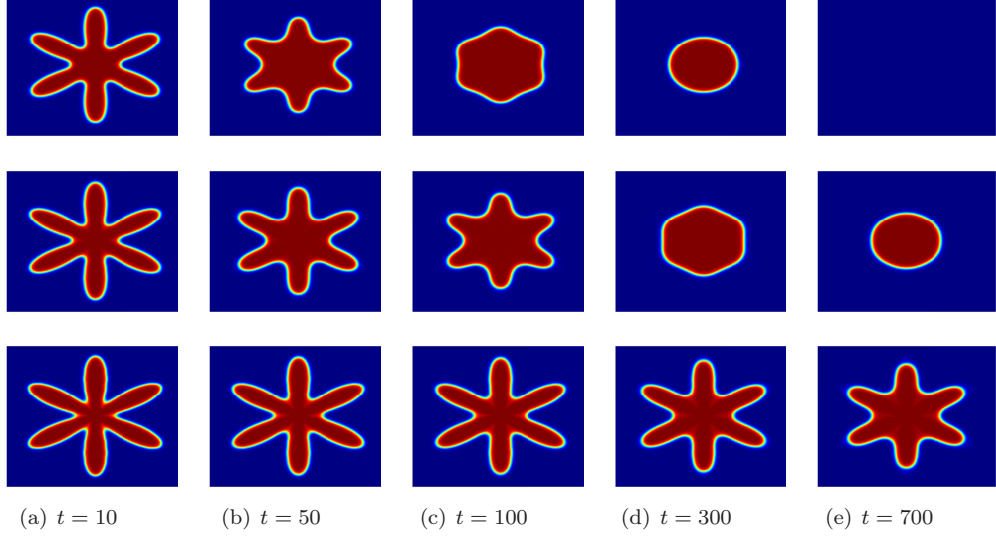


Figure 8: The dynamic snapshots of the numerical solution ϕ obtained by the $L1$ -sESAV scheme for the tFAC model with $\alpha = 0.9, 0.7, 0.4$ (from top to bottom, respectively)

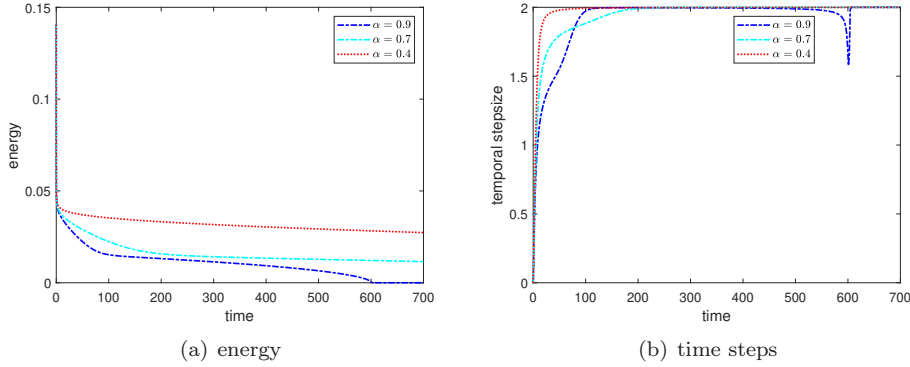


Figure 9: Time evolutions of the energy (left) and time steps (right) of the $L1$ -sESAV scheme for the tFAC model with $\alpha = 0.9, 0.7, 0.4$

3.5. 3D bubble merging

We finally consider the three-dimensional tFAC model with $m = 1$, $\varepsilon = 0.03$, and $\alpha = 0.5$. In this example, again only the double-well potential (2.2) is considered. The adaptive $L1$ -sESAV scheme is employed to simulate the 3D bubble merging with an initial condition $\phi_{\text{init}}(x, y, z) = \max\{\phi_1, \phi_2\}$ with

$$\phi_i = \tanh\left(\frac{0.2 - \sqrt{(x \pm 0.14)^2 + y^2 + z^2}}{\varepsilon}\right), \quad i = 1, 2.$$

In this test, we use $80 \times 80 \times 80$ uniform meshes in space to discretize the computational domain $\Omega = (-0.5, 0.5)^3$, and choose $\tau_{\max} = 1$, $\tau_{\min} = 0.01$, and $\eta = 10^7$ in the adaptive

time-stepping strategy (3.4). Figure 10 shows the iso-surfaces (value 0) of the numerical solution obtained by the $L1$ -sESAV scheme at different time instants, clearly illustrating that the two balls gradually shrink and merge into one smaller ball. Moreover, the discrete energy stability and MBP are well preserved by the numerical solution, as shown in Figures 11(a)–11(b). Finally, Figure 11(c) displays the history curves of the adaptive time steps, demonstrating the high efficiency of the time-adaptivity technique.

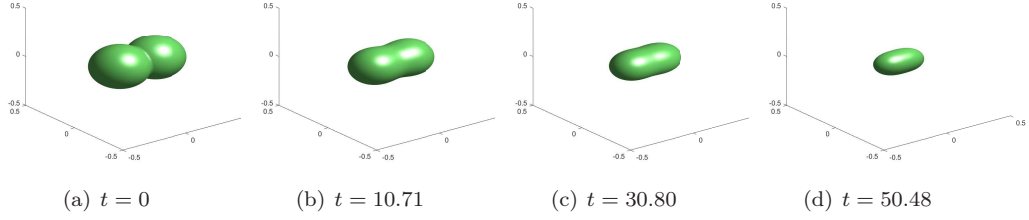


Figure 10: Plots of the iso-surfaces (value 0) of the numerical solution at different time instants obtained by the $L1$ -sESAV scheme for the tFAC model with $\alpha = 0.5$

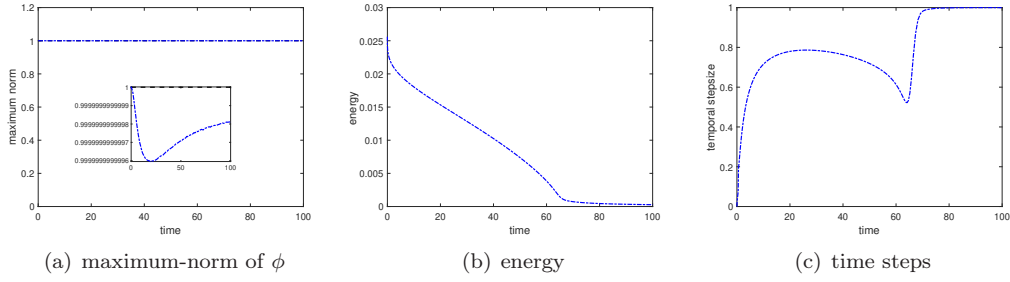


Figure 11: Time evolutions of the maximum norm (left), energy (middle), and time steps (right) for the $L1$ -sESAV scheme for the tFAC model with $\alpha = 0.5$

4. Stabilized $L2$ - 1_σ type ESAV schemes

In this section, we extend the ideas and derivations presented in Section 2 to the second-order $L2$ - 1_σ formula. Actually, the generalized approaches introduced below also enable the development of high-order numerical methods based on other discrete Caputo derivatives, such as the $L1_R$ formula [27] or the fast $L1$ formula [19]. For a given grid function $\{w^k\}$ with $k \geq 1$ and $0 < \varsigma < 1$, we define the off-set time level $t_{k-\varsigma} := (1 - \varsigma)t_k + \varsigma t_{k-1}$ and the weighted operator $w^{k-\varsigma} := (1 - \varsigma)w^k + \varsigma w^{k-1}$. Following [3, 25], we introduce the $L2$ - 1_σ formula on a nonuniform grid to approximate the Caputo fractional derivative at $t = t_{n-\varsigma}$ with $\varsigma := \alpha/2$

$${}_0^C D_t^\alpha w(t_{n-\varsigma}) \approx \tilde{\mathbb{D}}_\tau^\alpha w^n := \sum_{k=1}^n B_{n-k}^{(n)} \nabla_\tau w^k, \quad (4.1)$$

where the discrete convolution kernels $\{B_{n-k}^{(n)}\}$ are defined as follows: $B_0^{(1)} = a_0^{(1)}$ if $n = 1$ and for $n \geq 2$

$$B_{n-k}^{(n)} := \begin{cases} a_0^{(n)} + b_1^{(n)}/r_n, & k = n, \\ a_{n-k}^{(n)} + b_{n-k+1}^{(n)}/r_k - b_{n-k}^{(n)}, & 2 \leq k \leq n-1, \\ a_{n-1}^{(n)} - b_{n-1}^{(n)}, & k = 1, \end{cases} \quad (4.2)$$

with the discrete coefficients given by

$$a_{n-k}^{(n)} := \frac{1}{\tau_k} \int_{t_{k-1}}^{\min\{t_k, t_{n-\varsigma}\}} \omega_{1-\alpha}(t_{n-\varsigma} - s) ds, \quad 1 \leq k \leq n,$$

$$b_{n-k}^{(n)} := \frac{2}{\tau_k(\tau_k + \tau_{k+1})} \int_{t_{k-1}}^{t_k} (s - t_{k-\frac{1}{2}}) \omega_{1-\alpha}(t_{n-\varsigma} - s) ds, \quad 1 \leq k \leq n-1.$$

It is easy to check that $a_0^{(n)} = \frac{1}{\tau_n} \int_{t_{n-1}}^{t_{n-\varsigma}} \omega_{1-\alpha}(t_{n-\varsigma} - s) ds = \frac{(1-\varsigma)^{1-\alpha}}{\Gamma(2-\alpha)\tau_n^\alpha} > 0$. Besides, it is shown in [25, 26] that the discrete convolution kernels satisfy the following properties.

Lemma 4.1 ([26]). *Assume that the time-step ratio $r_k \geq 4/7$ for $2 \leq k \leq n$ holds. Then*

(i) *the discrete kernels $B_{n-k}^{(n)}$ fulfill $B_0^{(n)} \leq \frac{24}{11\tau_n} \int_{t_{n-1}}^{t_n} \omega_{1-\alpha}(t_n - s) ds$ and*

$$B_{n-k}^{(n)} \geq \frac{4}{11\tau_n} \int_{t_{n-1}}^{t_n} \omega_{1-\alpha}(t_n - s) ds = \frac{4}{11\Gamma(2-\alpha)\tau_n^\alpha}, \quad 1 \leq k \leq n;$$

(ii) *the discrete kernels $B_{n-k}^{(n)}$ are monotone, i.e., $B_{n-k+1}^{(n)} < B_{n-k}^{(n)}$ for $1 \leq k \leq n$;*

(iii) *and the first kernel $B_0^{(n)}$ is appropriately larger than the second one, i.e.,*

$$\frac{1-2\varsigma}{1-\varsigma} B_0^{(n)} - B_1^{(n)} > 0 \quad \text{for } n \geq 2.$$

Lemma 4.2 ([29]). *Assume that the time-step ratio $r_k \geq r_*(\alpha)$ for $2 \leq k \leq n$ holds, where $r_*(\alpha) \in (0.3865, 0.4037)$ for $\alpha \in (0, 1)$, then it holds*

$$(\nabla_\tau w^n) \tilde{\mathbb{D}}_\tau^\alpha w^n \geq \mathcal{G}[\nabla_\tau w^n] - \mathcal{G}[\nabla_\tau w^{n-1}] + \frac{\alpha a_0^{(n)}}{2-\alpha} (\nabla_\tau w^n)^2 \quad \text{for } n \geq 1,$$

where the nonnegative functional \mathcal{G} is defined by

$$\mathcal{G}[w^n] := \frac{1}{2} \sum_{j=1}^{n-1} (C_{n-j-1}^{(n)} - C_{n-j}^{(n)}) \left(\sum_{\ell=j+1}^n w^\ell \right)^2 + \frac{1}{2} C_{n-1}^{(n)} \left(\sum_{\ell=1}^n w^\ell \right)^2 \quad \text{for } n \geq 1,$$

and $\mathcal{G}[w^0] = 0$, with $C_0^{(n)} = 4(1-\alpha)a_0^{(n)}/(2-\alpha) + 2b_1^{(n)}/r_n$ and $C_{n-k}^{(n)} = B_{n-k}^{(n)}$.

4.1. Stabilized $L2-1_\sigma$ -ESAV scheme

Following the concept of $L1$ -sESAV scheme in Section 2, we apply the nonuniform $L2-1_\sigma$ formula (4.1) for the approximation of (2.6) to derive the stabilized second-order ESAV scheme (denoted as $L2-1_\sigma$ -sESAV):

Step 1. Let $\hat{\phi}^0 = \phi^0$. For $n = 1$, first solve a predicted solution $\hat{\phi}^1$ from the fully-implicit difference scheme:

$$\tilde{\mathbb{D}}_\tau^\alpha \hat{\phi}^1 := B_0^{(1)}(\hat{\phi}^1 - \phi^0) = m(\varepsilon^2 \Delta_h \hat{\phi}^{1-\varsigma} + f(\hat{\phi}^{1-\varsigma})), \quad (4.3)$$

where $\hat{\phi}^{1-\varsigma} := (1 - \varsigma)\hat{\phi}^1 + \varsigma\phi^0$, and let $V^{1-\varsigma} := V(g_h(\hat{\phi}^{1-\varsigma}, R^0))$, then find $\{\phi^1, R^1\} \in \mathbb{V}_h \times \mathbb{R}$ by

$$\tilde{\mathbb{D}}_\tau^\alpha \phi^1 = m(\varepsilon^2 \Delta_h \phi^{1-\varsigma} + V^{1-\varsigma} f(\hat{\phi}^{1-\varsigma}) - \kappa V^{1-\varsigma}(\phi^{1-\varsigma} - \hat{\phi}^{1-\varsigma})), \quad (4.4)$$

$$\mathbb{D}_\tau R^1 = V^{1-\varsigma} \langle -f(\hat{\phi}^{1-\varsigma}) + \kappa(\phi^{1-\varsigma} - \hat{\phi}^{1-\varsigma}), \mathbb{D}_\tau \phi^1 \rangle. \quad (4.5)$$

Step 2. For $n \geq 2$, given ϕ^{n-1} and ϕ^{n-2} , first predict a MBP-preserving solution $\hat{\phi}^n$ by (2.12) and let $\hat{\phi}^{n-\varsigma} := (1 - \varsigma)\hat{\phi}^n + \varsigma\phi^{n-1}$, $V^{n-\varsigma} := V(g_h(\hat{\phi}^{n-\varsigma}, R^{n-1}))$, then find $\{\phi^n, R^n\} \in \mathbb{V}_h \times \mathbb{R}$ such that

$$\tilde{\mathbb{D}}_\tau^\alpha \phi^n = m(\varepsilon^2 \Delta_h \phi^{n-\varsigma} + V^{n-\varsigma} f(\hat{\phi}^{n-\varsigma}) - \kappa V^{n-\varsigma}(\phi^{n-\varsigma} - \hat{\phi}^{n-\varsigma})), \quad (4.6)$$

$$\mathbb{D}_\tau R^n = V^{n-\varsigma} \langle -f(\hat{\phi}^{n-\varsigma}) + \kappa(\phi^{n-\varsigma} - \hat{\phi}^{n-\varsigma}), \mathbb{D}_\tau \phi^n \rangle. \quad (4.7)$$

Remark 5. As mentioned in Remark 2, the nonlinear scheme (4.3) in **Step 1** of the $L2-1_\sigma$ -sESAV scheme can be solved by performing the following simple iterative scheme with a given termination error tol :

$$B_0^{(1)}(\hat{\phi}_{(\mathfrak{s})}^1 - \phi^0) = m(\varepsilon^2 \Delta_h \hat{\phi}_{(\mathfrak{s})}^{1-\varsigma} + f(\hat{\phi}_{(\mathfrak{s}-1)}^{1-\varsigma}) - \kappa(\hat{\phi}_{(\mathfrak{s})}^{1-\varsigma} - \hat{\phi}_{(\mathfrak{s}-1)}^{1-\varsigma})) \quad \text{for } \mathfrak{s} \geq 1, \quad (4.8)$$

where $\hat{\phi}_{(\ell)}^{1-\varsigma} = (1 - \varsigma)\hat{\phi}_{(\ell)}^1 + \varsigma\phi^0$ with $\ell = \mathfrak{s} - 1, \mathfrak{s}$, and the initial iteration value is set as $\hat{\phi}_{(0)}^1 = \phi^0$. Therefore, the practical implementation of the $L2-1_\sigma$ -sESAV scheme can refer to that of the $L1$ -sESAV scheme described in Algorithm 1. The following Theorem 4.3 demonstrates that the nonlinear scheme (4.3) is MBP-preserving and uniquely solvable. Following similar mathematical induction argument as in Theorem 2.5, we can prove Theorem 4.3, see Appendix B for details.

Theorem 4.3. Assume that the condition in Lemma 4.1 holds and $\kappa \geq \|f'\|_{C[-\beta, \beta]}$. If the first level time-step τ_1 is sufficiently small such that

$$\tau_1 \leq \sqrt[3]{4/(11\varsigma m(\kappa + 4\varepsilon^2/h^2)\Gamma(2 - \alpha))}, \quad (4.9)$$

the iterative scheme (4.8) preserves the MBP for $\{\hat{\phi}_{(\mathfrak{s})}^1\}$. Furthermore, if τ_1 satisfies

$$\tau_1 \leq \sqrt[3]{4/(11\kappa(1 - \varsigma)m\Gamma(2 - \alpha))}, \quad (4.10)$$

then the iterative scheme (4.8) converges to the unique solution $\hat{\phi}^1$ of the nonlinear scheme (4.3) in the maximum norm satisfying $\|\hat{\phi}^1\|_\infty \leq \beta$.

Remark 6. The unique solvability of the $L2-1_\sigma$ -sESAV scheme can be discussed similarly as Theorem 2.5, by equivalently rewriting (4.4)–(4.5) and (4.6)–(4.7) in a uniform form:

$$\begin{aligned} & [(B_0^{(n)} + \kappa(1 - \varsigma)mV^{n-\varsigma})I - (1 - \varsigma)m\varepsilon^2\Delta_h]\phi^n \\ &= [(B_0^{(n)} - \kappa\varsigma mV^{n-\varsigma})I + \varsigma m\varepsilon^2\Delta_h]\phi^{n-1} \\ &+ \sum_{k=1}^{n-1} B_{n-k}^{(n)} \nabla_\tau \phi^k + mV^{n-\varsigma} (\kappa \hat{\phi}^{n-\varsigma} + f(\hat{\phi}^{n-\varsigma})), \end{aligned} \quad (4.11)$$

$$R^n = R^{n-1} + V^{n-\varsigma} \langle -f(\hat{\phi}^{n-\varsigma}) + \kappa(\phi^{n-\varsigma} - \hat{\phi}^{n-\varsigma}), \phi^n - \phi^{n-1} \rangle. \quad (4.12)$$

Since $B_0^{(n)} > 0$, it can be verified that the coefficient matrix of (4.11) is symmetric and positive definite. In fact, it is also strictly diagonally dominant.

4.2. Discrete energy stability and MBP

The following two theorems establish the discrete energy stability and MBP for the proposed $L2-1_\sigma$ -sESAV scheme (4.3)–(4.7).

Theorem 4.4. *Assume that the conditions in Lemma 4.2 and Theorem 4.3 hold, the $L2-1_\sigma$ -sESAV scheme (4.3)–(4.7) is unconditionally energy-stable in the sense that $\mathcal{E}_h[\phi^n, R^n] \leq \mathcal{E}_h[\phi^0, R^0]$ for $n \geq 1$.*

Proof. Let $n = k$ in (4.6) and take the inner product with $\nabla_\tau \phi^k = \phi^k - \phi^{k-1}$. We then combine the resulting equation with (4.12) to derive

$$R^k - R^{k-1} - \varepsilon^2 \langle \Delta_h \phi^{k-\varsigma}, \phi^k - \phi^{k-1} \rangle = -\frac{1}{m} \langle \tilde{\mathbb{D}}_\tau^\alpha \phi^k, \phi^k - \phi^{k-1} \rangle. \quad (4.13)$$

It is straightforward to verify that

$$((1 - \sigma)a + \sigma b)(a - b) = a(a - b) - \sigma(a - b)^2 = \frac{1}{2}a^2 - \frac{1}{2}b^2 + \frac{1 - 2\sigma}{2}(a - b)^2, \quad \forall \sigma \in \mathbb{R}. \quad (4.14)$$

Thus, by taking $\sigma = \varsigma = \alpha/2$ with $\alpha \in (0, 1)$ in (4.14), the third left-hand side term of (4.13) can be estimated by

$$-\varepsilon^2 \langle \Delta_h \phi^{k-\varsigma}, \phi^k - \phi^{k-1} \rangle \geq \frac{\varepsilon^2}{2} \|\nabla_h \phi^k\|^2 - \frac{\varepsilon^2}{2} \|\nabla_h \phi^{k-1}\|^2. \quad (4.15)$$

Inserting (4.15) into (4.13), we get

$$\mathcal{E}_h[\phi^k, R^k] - \mathcal{E}_h[\phi^{k-1}, R^{k-1}] \leq -\frac{1}{m} \langle \tilde{\mathbb{D}}_\tau^\alpha \phi^k, \phi^k - \phi^{k-1} \rangle, \quad k \geq 2. \quad (4.16)$$

Similarly, it follows from (4.4) and (4.12) that (4.16) also holds for $k = 1$.

Now, we sum the above inequality (4.16) from $k = 1$ to n to derive

$$\begin{aligned} \mathcal{E}_h[\phi^n, R^n] - \mathcal{E}_h[\phi^0, R^0] &\leq -\frac{1}{m} \sum_{k=1}^n (\langle \mathcal{G}[\nabla_\tau \phi^k], 1 \rangle - \langle \mathcal{G}[\nabla_\tau \phi^{k-1}], 1 \rangle) \\ &= -\frac{1}{m} \langle \mathcal{G}[\nabla_\tau \phi^n], 1 \rangle \leq 0, \end{aligned}$$

where Lemma 4.2 has been used in the first inequality. The proof is completed. \square

Theorem 4.5. Assume that the conditions in Theorem 4.3 hold. Furthermore, if the time-step satisfies

$$\tau_n \leq \sqrt[3]{4/(11(1-\varsigma)m(4\varepsilon^2/h^2 + \kappa K_2)\Gamma(2-\alpha))}, \quad n \geq 1, \quad (4.17)$$

where K_2 is the upper bound of $V(\cdot)$, the L2-1 $_{\sigma}$ -sESAV scheme (4.3)–(4.7) preserves the MBP for $\{\phi^n\}$, that is,

$$\text{if } \|\phi^0\|_{\infty} \leq \beta \implies \|\phi^n\|_{\infty} \leq \beta, \quad \forall n \geq 1.$$

Proof. For $n = 1$, it follows from (4.11) that

$$[(B_0^{(1)} + \kappa(1-\varsigma)mV^{1-\varsigma})I - (1-\varsigma)m\varepsilon^2\Delta_h]\phi^1 = \mathbf{M}_2^1\phi^0 + mV^{1-\varsigma}(\kappa\hat{\phi}^{1-\varsigma} + f(\hat{\phi}^{1-\varsigma})), \quad (4.18)$$

with $\mathbf{M}_2^1 = (B_0^{(1)} - \kappa\varsigma mV^{1-\varsigma})I + \varsigma m\varepsilon^2\Delta_h$. Theorem 4.3 demonstrates that $\|\hat{\phi}^1\|_{\infty} \leq \beta$ when τ_1 satisfies (4.9)–(4.10), thereby ensuring that $\|\hat{\phi}^{1-\varsigma}\|_{\infty} \leq \beta$. Then, the application of Lemmas 2.3–2.4 leads to

$$(B_0^{(1)} + \kappa(1-\varsigma)mV^{1-\varsigma})\|\phi^1\|_{\infty} \leq \|\mathbf{M}_2^1\phi^0\|_{\infty} + \kappa mV^{1-\varsigma}\beta. \quad (4.19)$$

Moreover, if (4.17) holds for $n = 1$, all elements of \mathbf{M}_2^1 are nonnegative, and thus

$$\|\mathbf{M}_2^1\|_{\infty} = B_0^{(1)} - \kappa\varsigma mV^{1-\varsigma},$$

which yields $\|\mathbf{M}_2^1\phi^0\|_{\infty} \leq \|\mathbf{M}_2^1\|_{\infty} \|\phi^0\|_{\infty} \leq B_0^{(1)}\beta - \kappa\varsigma mV^{1-\varsigma}\beta$. Inserting this estimate into (4.19), we obtain $\|\phi^1\|_{\infty} \leq \beta$.

For $2 \leq n \leq N$, suppose that $\|\phi^k\|_{\infty} \leq \beta$ for $0 \leq k \leq n-1$. It follows from (2.12) and the definition of $\hat{\phi}^{n-\varsigma}$ that $\|\hat{\phi}^{n-\varsigma}\|_{\infty} \leq \beta$. Thus, it remains to verify that $\|\phi^n\|_{\infty} \leq \beta$. Noting that (4.1) can be expressed as

$$\tilde{\mathbb{D}}_{\tau}^{\alpha}\phi^n = B_0^{(n)}\phi^n - (B_0^{(n)} - B_1^{(n)})\phi^{n-1} - \Xi^{n-2}(\phi),$$

where

$$\Xi^{n-2}(\phi) := \sum_{k=1}^{n-2} (B_{n-k-1}^{(n)} - B_{n-k}^{(n)})\phi^k + B_{n-1}^{(n)}\phi^0.$$

Then, (4.6) can be rewritten as

$$\begin{aligned} & [(B_0^{(n)} + \kappa(1-\varsigma)mV^{n-\varsigma})I - (1-\varsigma)m\varepsilon^2\Delta_h]\phi^n \\ &= \mathbf{M}_2^n\phi^{n-1} + \Xi^{n-2}(\phi) + mV^{n-\varsigma}(\kappa\hat{\phi}^{n-\varsigma} + f(\hat{\phi}^{n-\varsigma})), \end{aligned} \quad (4.20)$$

where the matrix

$$\mathbf{M}_2^n := (B_0^{(n)} - B_1^{(n)} - \kappa\varsigma mV^{n-\varsigma})I + \varsigma m\varepsilon^2\Delta_h.$$

Under the condition (4.17), and Lemma 4.1 (i) and (iii), we see

$$B_0^{(n)} - B_1^{(n)} > \frac{\varsigma}{1-\varsigma}B_0^{(n)} \geq \frac{4\varsigma\tau_n^{-\alpha}}{11(1-\varsigma)\Gamma(2-\alpha)} \geq \kappa\varsigma mV^{n-\varsigma} + \frac{4\varsigma m\varepsilon^2}{h^2},$$

which further means that all elements of \mathbf{M}_2^n are nonnegative and

$$\|\mathbf{M}_2^n\|_\infty = B_0^{(n)} - B_1^{(n)} - \kappa\varsigma m V^{n-\varsigma}.$$

Consequently, the hypothesis $\|\phi^{n-1}\|_\infty \leq \beta$ yields

$$\|\mathbf{M}_2^n \phi^{n-1}\|_\infty \leq \|\mathbf{M}_2^n\|_\infty \|\phi^{n-1}\|_\infty \leq (B_0^{(n)} - B_1^{(n)} - \kappa\varsigma m V^{n-\varsigma})\beta. \quad (4.21)$$

Moreover, the positivity and monotonicity of the discrete kernels $\{B_{n-k}^{(n)}\}$, along with the assumption that $\|\phi^k\|_\infty \leq \beta, 0 \leq k \leq n-1$, lead to

$$\|\Xi^{n-2}(\phi)\|_\infty \leq \sum_{k=1}^{n-2} (B_{n-k-1}^{(n)} - B_{n-k}^{(n)}) \|\phi^k\|_\infty + B_{n-1}^{(n)} \|\phi^0\|_\infty \leq B_1^{(n)} \beta. \quad (4.22)$$

Therefore, collecting the estimates (4.21)–(4.22) and using Lemmas 2.3–2.4, it follows from (4.20) that

$$\begin{aligned} & (B_0^{(n)} + \kappa(1-\varsigma)mV^{n-\varsigma})\|\phi^n\|_\infty \\ & \leq \|[(B_0^{(n)} + \kappa(1-\varsigma)mV^{n-\varsigma})I - (1-\varsigma)m\varepsilon^2\Delta_h]\phi^n\|_\infty \\ & = \|\mathbf{M}_2^n \phi^{n-1} + \Xi^{n-2}(\phi) + mV^{n-\varsigma}(\kappa\hat{\phi}^{n-\varsigma} + f(\hat{\phi}^{n-\varsigma}))\|_\infty \\ & \leq B_0^{(n)}\beta + \kappa(1-\varsigma)mV^{n-\varsigma}\beta. \end{aligned} \quad (4.23)$$

This immediately implies $\|\phi^n\|_\infty \leq \beta$ and completes the proof. \square

4.3. Novel unbalanced stabilized $L2$ -1 σ -sESAV scheme

In cases that the auxiliary functional $V(\cdot)$ satisfies the assumptions (A1)–(A3) with $K_2 = 1$, we can further improve the $L2$ -1 σ -sESAV scheme by introducing a novel unbalanced stabilization term

$$\kappa(\phi^{n-\varsigma} - V^{n-\varsigma}\hat{\phi}^{n-\varsigma}), \quad n \geq 1. \quad (4.24)$$

The imbalance, reflected by $V^{n-\varsigma} \neq 1$ for $n \geq 1$ generally, is beneficial for the preservation of MBP especially for large time step, see Remark 7 and Figures 12–13 in subsection 4.4.2. Using the modified stabilization term (4.24), a novel unbalanced $L2$ -1 σ -sESAV scheme is proposed as follows:

Step 1. Let $\hat{\phi}^0 = \phi^0$. For $n = 1$, first solve a predicted solution $\hat{\phi}^1$ from the fully-implicit difference scheme (4.3), then find $\{\phi^1, R^1\} \in \mathbb{V}_h \times \mathbb{R}$ by

$$\tilde{\mathbb{D}}_\tau^\alpha \phi^1 = m(\varepsilon^2 \Delta_h \phi^{1-\varsigma} + V^{1-\varsigma} f(\hat{\phi}^{1-\varsigma}) - \kappa(\phi^{1-\varsigma} - V^{1-\varsigma} \hat{\phi}^{1-\varsigma})), \quad (4.25)$$

$$\mathbb{D}_\tau R^1 = -V^{1-\varsigma} \langle f(\hat{\phi}^{1-\varsigma}), \mathbb{D}_\tau \phi^1 \rangle + \kappa \langle \phi^{1-\varsigma} - V^{1-\varsigma} \hat{\phi}^{1-\varsigma}, \mathbb{D}_\tau \phi^1 \rangle. \quad (4.26)$$

Step 2. For $n \geq 2$, given ϕ^{n-1} and ϕ^{n-2} , first predict a MBP-preserving solution $\hat{\phi}^n$ by (2.12), then find $\{\phi^n, R^n\} \in \mathbb{V}_h \times \mathbb{R}$ such that

$$\tilde{\mathbb{D}}_\tau^\alpha \phi^n = m(\varepsilon^2 \Delta_h \phi^{n-\varsigma} + V^{n-\varsigma} f(\hat{\phi}^{n-\varsigma}) - \kappa(\phi^{n-\varsigma} - V^{n-\varsigma} \hat{\phi}^{n-\varsigma})), \quad (4.27)$$

$$\mathbb{D}_\tau R^n = -V^{n-\varsigma} \langle f(\hat{\phi}^{n-\varsigma}), \mathbb{D}_\tau \phi^n \rangle + \kappa \langle \phi^{n-\varsigma} - V^{n-\varsigma} \hat{\phi}^{n-\varsigma}, \mathbb{D}_\tau \phi^n \rangle. \quad (4.28)$$

Following the proofs of Theorems 4.4–4.5, together with Lemmas 4.1–4.3, the preservation of energy stability and MBP for the unbalanced $L2$ -1 σ -sESAV scheme can be established in a similar manner.

Theorem 4.6. Assume that the conditions in Lemma 4.2 and Theorem 4.3 hold, the unbalanced $L2$ -1 σ -sESAV scheme (4.25)–(4.28) is unconditionally energy-stable in the sense that $\mathcal{E}_h[\phi^n, R^n] \leq \mathcal{E}_h[\phi^0, R^0]$ for $n \geq 1$.

Theorem 4.7. Assume that the conditions in Theorem 4.3 hold. If the time-step satisfies

$$\tau_n \leq \sqrt[3]{4/(11(1-\varsigma)m(4\varepsilon^2/h^2 + \kappa)\Gamma(2-\alpha))}, \quad n \geq 1, \quad (4.29)$$

the unbalanced $L2$ -1 σ -sESAV scheme (4.25)–(4.28) preserves the MBP for $\{\phi^n\}$, that is,

$$\text{if } \|\phi^0\|_\infty \leq \beta \implies \|\phi^n\|_\infty \leq \beta, \quad \forall n \geq 1.$$

Proof. Together with a similar treatment to (4.18)–(4.23), we conclude from (4.25) and (4.27) that

$$(B_0^{(n)} + \kappa(1-\varsigma)m)\|\phi^n\|_\infty \leq B_0^{(n)}\beta + \kappa(1-\varsigma)m\beta + \mathcal{P}^n, \quad n \geq 1, \quad (4.30)$$

under the condition (4.29), where $\mathcal{P}^n := \kappa m(V^{n-\varsigma} - 1)\beta$. The assumption (A2) with $K_2 = 1$ ensures that $\mathcal{P}^n \leq 0$, thereby further guarantees that the unbalanced $L2$ -1 σ -sESAV scheme preserves the MBP. \square

Remark 7. The result (4.30) directly leads to

$$\|\phi^n\|_\infty \leq \beta + \frac{\mathcal{P}^n}{B_0^{(n)} + \kappa(1-\varsigma)m}.$$

From assumption (A3), we know that $g_h(\hat{\phi}^{n-\varsigma}, R^{n-1})$ and $V^{n-\varsigma}$ may deviate significantly from 1 for a large time step. In this sense, the negative term $\frac{\mathcal{P}^n}{B_0^{(n)} + \kappa(1-\varsigma)m}$ can be considered as a penalty term to generate solutions with smaller L^∞ -norm. However, no such term exists in the standard $L2$ -1 σ -sESAV scheme, indicating that, compared to the standard one, the proposed unbalanced $L2$ -1 σ -sESAV scheme is more effective in preserving the MBP, see also the numerical results in Figures 12–13.

4.4. Numerical experiments

This subsection is devoted to numerical tests of both the $L2$ -1 σ -sESAV and unbalanced $L2$ -1 σ -sESAV schemes. Note that for the $L2$ -1 σ type methods, a time-step ratio constraint $r_k \geq 4/7$ is required to preserve the discrete energy stability (cf. Theorems 4.4 and 4.6) and MBP (cf. Theorems 4.5 and 4.7). Thus, in the numerical simulations, the following modified adaptive time-stepping strategy

$$\tau_k = \max \left\{ \max \left\{ \tau_{\min}, \frac{\tau_{\max}}{\sqrt{1 + \eta |\partial_\tau E^{k-1}|^2}} \right\}, r_{\min} \tau_{k-1} \right\} \quad (4.31)$$

is adopted, where $r_{\min} \geq 4/7$ is a user-defined constant.

4.4.1. Temporal convergence

We first verify the temporal accuracy of both the balanced and unbalanced $L2-1_\sigma$ -sESAV schemes, and the numerical results are obtained by solving the exterior-forced problem (3.5) with a fixed fractional order $\alpha = 0.8$. For different regularity parameters $\iota = 0.3, 0.5$ and 0.8 , the mesh grading parameter is set to be $\gamma = 2/\iota$ such that the theoretical convergence order is $\min\{2, \gamma\iota\} = 2$. The other setup is the same as in subsection 3.1. Numerical results for the two type potentials are listed in Tables 4–5, from which we can clearly observe that (i) both methods exhibit second-order temporal accuracy as expected; and (ii) they generate numerical solutions with the same magnitude accuracy.

Table 4: Time accuracy of the $L2-1_\sigma$ -sESAV schemes with $\alpha = 0.8$ and $\gamma = 2/\iota$: the double-well potential

method	N	$\iota = 0.3$		$\iota = 0.5$		$\iota = 0.8$	
		$e(N)$	Order	$e(N)$	Order	$e(N)$	Order
$L2-1_\sigma$ -sESAV scheme	20	1.95×10^{-2}	—	5.35×10^{-3}	—	8.98×10^{-4}	—
	40	4.99×10^{-3}	1.97	1.38×10^{-3}	1.96	1.85×10^{-4}	2.28
	80	1.25×10^{-3}	2.00	3.46×10^{-4}	1.99	4.41×10^{-5}	2.07
	160	3.18×10^{-4}	1.98	8.66×10^{-5}	2.00	1.11×10^{-5}	1.99
	320	7.94×10^{-5}	2.00	2.17×10^{-5}	2.00	2.79×10^{-6}	1.99
unbalanced $L2-1_\sigma$ -sESAV scheme	20	1.95×10^{-2}	—	5.40×10^{-3}	—	1.64×10^{-3}	—
	40	4.99×10^{-3}	1.97	1.38×10^{-3}	1.97	2.68×10^{-4}	2.62
	80	1.25×10^{-3}	2.00	3.46×10^{-4}	1.99	5.73×10^{-5}	2.22
	160	3.18×10^{-4}	1.98	8.66×10^{-5}	2.00	1.32×10^{-5}	2.12
	320	7.94×10^{-5}	2.00	2.17×10^{-5}	2.00	2.84×10^{-6}	2.22
$\min\{2, \gamma\iota\}$			2.00	2.00		2.00	

Table 5: Time accuracy of the $L2-1_\sigma$ -sESAV schemes with $\alpha = 0.8$ and $\gamma = 2/\iota$: the Flory–Huggins potential

method	N	$\iota = 0.3$		$\iota = 0.5$		$\iota = 0.8$	
		$e(N)$	Order	$e(N)$	Order	$e(N)$	Order
$L2-1_\sigma$ -sESAV scheme	20	1.93×10^{-2}	—	5.19×10^{-3}	—	6.28×10^{-4}	—
	40	4.97×10^{-3}	1.96	1.36×10^{-3}	1.93	1.65×10^{-4}	1.93
	80	1.25×10^{-3}	1.99	3.46×10^{-4}	1.98	4.37×10^{-5}	1.92
	160	3.18×10^{-4}	1.98	8.66×10^{-5}	2.00	1.11×10^{-5}	1.98
	320	7.94×10^{-5}	2.00	2.17×10^{-5}	2.00	2.79×10^{-6}	1.98
unbalanced $L2-1_\sigma$ -sESAV scheme	20	1.97×10^{-2}	—	5.21×10^{-3}	—	2.40×10^{-3}	—
	40	4.98×10^{-3}	1.98	1.36×10^{-3}	1.93	4.33×10^{-4}	2.47
	80	1.25×10^{-3}	1.99	3.46×10^{-4}	1.98	8.17×10^{-5}	2.41
	160	3.18×10^{-4}	1.98	8.66×10^{-5}	2.00	1.85×10^{-5}	2.14
	320	7.94×10^{-5}	2.00	2.17×10^{-5}	2.00	4.00×10^{-6}	2.21
$\min\{2, \gamma\iota\}$			2.00	2.00		2.00	

4.4.2. Effectiveness of the unbalanced stabilization term

The coarsening dynamics of the tFAC model (1.1) is examined with $\alpha = 0.9$, $m = 1$, and $\varepsilon = 0.01$. We adopt a 128^2 spatial mesh to discretize the spatial domain $\Omega = (0, 1)^2$,

and give the initial value by random numbers uniformly distributed between -0.8 and 0.8 at each grid point, see Figure 1.

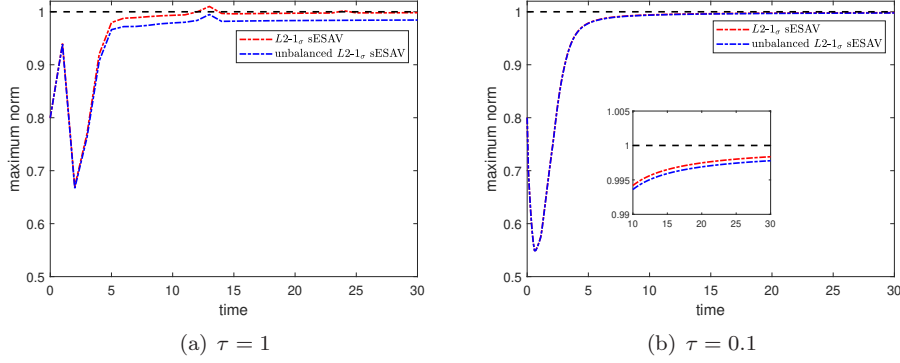


Figure 12: Time evolutions of the maximum norm and energy of simulated solutions computed by the $L2-1_\sigma$ -sESAV scheme with different stabilization terms: the double-well potential

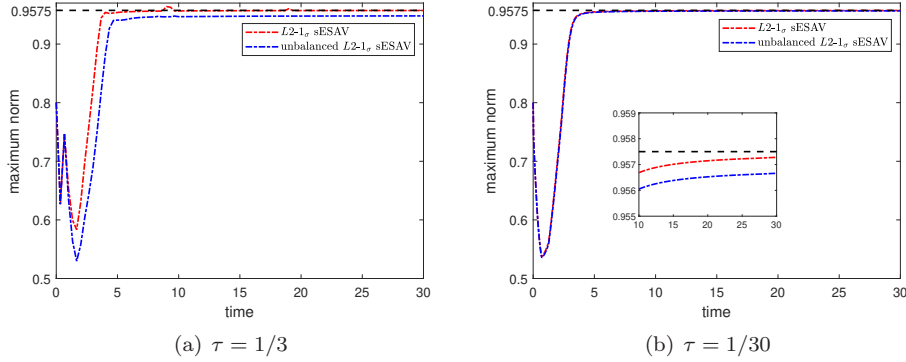


Figure 13: Time evolutions of the maximum norm and energy of simulated solutions computed by the $L2-1_\sigma$ -sESAV scheme with different stabilization terms: the Flory–Huggins potential

For special choice $V(\cdot)$ in (3.1), it deduces from Theorems 4.5 and 4.7 that $\tau \leq 0.1044$ for the double-well potential and $\tau \leq 0.0646$ for the Flory–Huggins potential are required to preserve the discrete MBP on uniform temporal grids. Note that these conditions are only sufficient but not necessary. Therefore, in the following tests, two different types of temporal grids (one satisfies the condition, while the other violates it) are employed for each potential, i.e., $\tau = 1, 0.1$ for the double-well case, and $\tau = 1/3, 1/30$ for the Flory–Huggins case. The coarsening dynamics are tested using the two $L2-1_\sigma$ -sESAV schemes with different stabilization terms. Numerical results for both the double-well potential and Flory–Huggins potential are depicted in Figures 12 and 13, respectively. As illustrated, the unbalanced $L2-1_\sigma$ -sESAV scheme can preserve the discrete MBP on both temporal grids, whereas the solutions of the standard one exceed the maximum-bound β when using the larger time step, see Figures 12(a) and 13(a). This demonstrates the effectiveness and excellence of the proposed unbalanced stabilization term in preserving discrete MBP.

4.4.3. Long-term coarsening dynamics simulations

The unbalanced $L2-1_\sigma$ -sESAV scheme has demonstrated superior reliability in preserving the MBP compared to the standard scheme, making it the preferred choice for simulating long-term coarsening dynamics governed by the tFAC model (1.1), particularly for extended time scales up to $T = 2000$ in the following test. Moreover, to improve the computational efficiency without sacrificing accuracy in the simulation, a mixed adaptive time-stepping strategy (3.2) and (4.31) with $\hat{T} = 0.5$ and $\hat{N} = 30$ is employed. Here we set $m = 1$, $\varepsilon = 0.01$, $r_{\min} = 4/7$, and $\eta = 10^7$, and $(\tau_{\min}, \tau_{\max}) = (0.1, 1)$ for the double-well potential and $(\tau_{\min}, \tau_{\max}) = (1/30, 1/3)$ for the Flory–Huggins potential. The random initial values and spatial partition are the same as aforementioned.

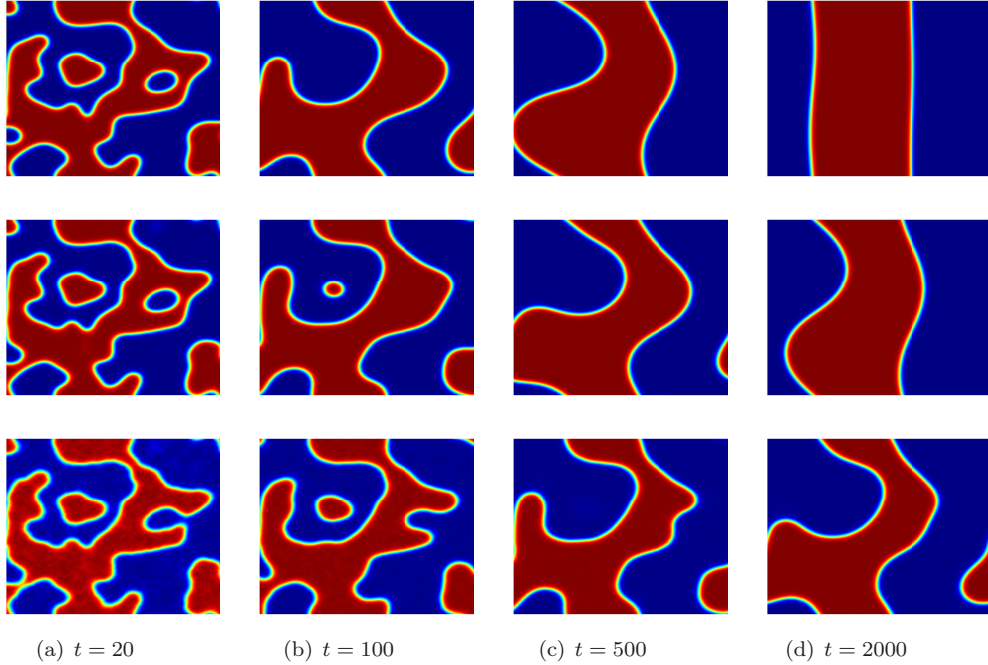


Figure 14: The dynamic snapshots of the numerical solution ϕ obtained by the unbalanced $L2-1_\sigma$ -sESAV scheme with $\alpha = 0.9, 0.7, 0.4$ (from top to bottom, respectively): the double-well potential

For the double-well potential, the profiles of coarsening dynamics with different fractional orders $\alpha = 0.9, 0.7$ and 0.4 are depicted in Figure 14, where snapshots are taken at times $t = 20, 100, 500$, and 2000 , respectively. It is clearly observed that the coarsening speed governed by the tFAC equation depends heavily on the fractional order α and smaller values of α require much longer time to reach the steady state. Moreover, Figure 15(a)–15(b) demonstrate that the proposed unbalanced $L2-1_\sigma$ -sESAV scheme with the adaptive time-stepping strategy successfully preserves both the discrete energy stability and MBP, and Figure 15(c) further shows that the time steps are accurately and effectively selected to capture the energy variations in the adaptive method. For the Flory–Huggins potential, the corresponding numerical results are presented in Figures 16–17, and similar conclusions can be also drawn.

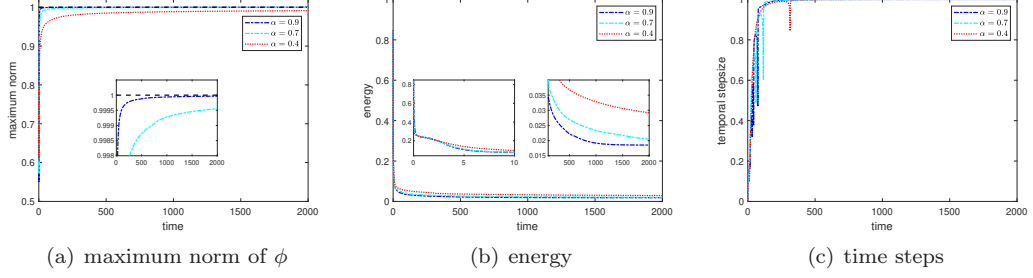


Figure 15: Time evolutions of the maximum norm (left), energy (middle), and time steps (right) for the unbalanced $L2-1_\sigma$ -sESAV scheme with $\alpha = 0.9, 0.7, 0.4$: the double-well potential

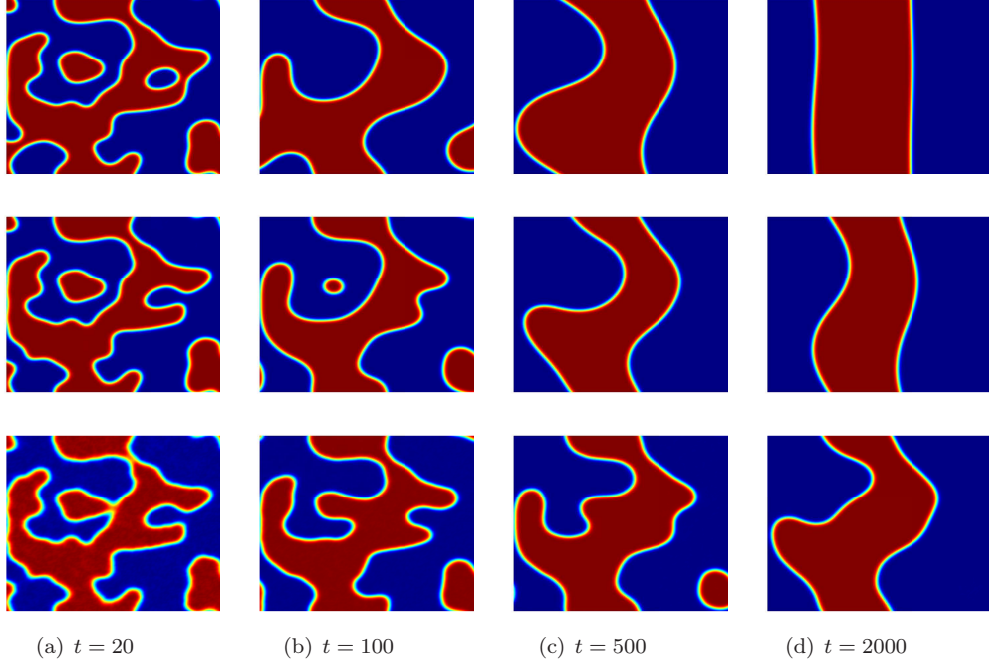


Figure 16: The dynamic snapshots of the numerical solution ϕ obtained by the unbalanced $L2-1_\sigma$ -sESAV scheme with $\alpha = 0.9, 0.7, 0.4$ (from top to bottom, respectively): the Flory–Huggins potential

5. Concluding remarks

In this paper, we first established the MBP for the tFAC model (1.1) with different nonlinear potentials. Subsequently, we developed and analyzed a linear stabilized nonuniform time-stepping scheme, referred to as the $L1$ -sESAV scheme, in which an essential auxiliary functional was introduced to ensure that the first-order approximation of the SAV does not compromise the temporal accuracy of the phase function. This treatment is critical for deriving unconditional energy stability of nonuniform time-stepping linear scheme. Moreover, the non-negativity of this novel auxiliary functional also allows for the design of a stabilization term that effectively controls the nonlinear term, which together

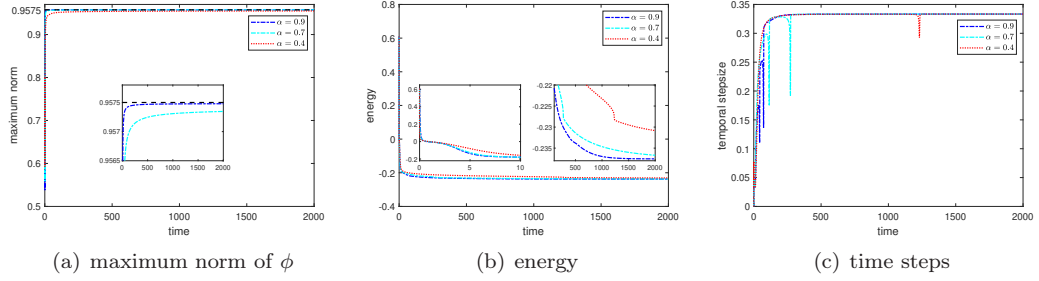


Figure 17: Time evolutions of the maximum norm (left), energy (middle), and time steps (right) for the unbalanced $L2-1_\sigma$ -sESAV scheme with $\alpha = 0.9, 0.7, 0.4$: the Flory–Huggins potential

with a newly developed prediction strategy guarantees the discrete MBP-preservation. To the best of our knowledge, this is the first $(2 - \alpha)$ th order $L1$ -type linear scheme with unconditional preservation of the energy stability and MBP.

Building on these ideas, we further established a linear second-order scheme, termed the $L2-1_\sigma$ -sESAV scheme, which can preserve the energy stability unconditionally and MBP conditionally. To enhance the discrete MBP preservation for large time steps, we also introduced an improved unbalanced stabilization term by imposing appropriate boundedness and monotonicity assumptions on the auxiliary functional, and then an unbalanced $L2-1_\sigma$ -sESAV scheme was developed and discussed. Numerical simulations for the two- and three-dimensional tFAC models with either the double-well potential or the Flory–Huggins potential suggest the satisfactory and high effectiveness of the proposed methods. Finally, we claim that the ideas and derivations presented in current paper can also be extended to other discrete Caputo derivatives, such as the $L1_R$ formula and the fast versions of $L1$ and $L2-1_\sigma$ formulas.

CRedit authorship contribution statement

Bingyin Zhang : Methodology, Formal analysis, Software, Writing-Original draft.
Hong Wang : Conceptualization, Writing-Reviewing and Editing, Funding acquisition.
Hongfei Fu : Methodology, Conceptualization, Supervision, Writing-Reviewing and Editing, Funding acquisition.

Declaration of competing interest

The authors declare that they have no known competing financial interests or personal relationships that could have appeared to influence the work reported in this paper.

Data availability

A free github repository contains the Matlab code employed, which can be accessed through the following link: <https://github.com/HFu20/time-Fractional-Allen-Cahn/tree/sESAV-MBP>.

Acknowledgements

This work was supported in part by the National Natural Science Foundation of China (Nos. 11971482, 12131014), by the Shandong Provincial Natural Science Foundation (No. ZR2024MA023), by the Fundamental Research Funds for the Central Universities (Nos. 202264006, 202461103), by the OUC Scientific Research Program for Young Talented Professionals, and by the National Science Foundation (Nos. DMS-2012291, DMS-2245097).

Appendix A. Proof of Lemma 2.2

The integral version of Taylor's theorem gives

$$\mathcal{R}^n[v] = (1 + r_n) \int_{t_{n-1}}^{t_n} v_{ss}(s)(t_{n-1} - s)ds + r_n \int_{t_{n-2}}^{t_n} v_{ss}(s)(s - t_{n-2})ds. \quad (\text{A.1})$$

Under the regularity assumption, one has

$$\begin{aligned} \left| (1 + r_n) \int_{t_{n-1}}^{t_n} v_{ss}(s)(t_{n-1} - s)ds \right| &\leq C_v t_{n-1}^{\iota-2} \tau_n^2, \quad 2 \leq n \leq N, \\ \left| r_n \int_{t_{n-2}}^{t_n} v_{ss}(s)(s - t_{n-2})ds \right| &\leq C_v t_{n-2}^{\iota-2} (\tau_{n-1} + \tau_n)^2, \quad 3 \leq n \leq N. \end{aligned}$$

Specifically, when $n = 2$, the second right-hand side term of (A.1) can be estimated by

$$\left| r_2 \int_{t_0}^{t_2} s v_{ss}(s)ds \right| \leq C_v \int_{t_0}^{t_2} s + s^{\iota-1} ds \leq C_v (\tau_1 + \tau_2)^\iota / \iota.$$

Inserting the above estimates into (A.1) completes the proof of (2.16).

In particular, when the graded temporal grids are used, we recall the conclusion in [32] that there exists a constant $C_\gamma > 0$ such that $\tau_k \leq C_\gamma t_k^{1-1/\gamma} N^{-1}$ and $t_k \leq C_\gamma t_{k-1}$ for $2 \leq k \leq N$, which further implies $\tau_1 + \tau_2 \leq 2\tau_2 \leq C'_\gamma N^{-\gamma}$ and thus $(\tau_1 + \tau_2)^\iota \leq C'_\gamma N^{-\gamma\iota}$. Denote $\zeta = \min\{2, \gamma\iota\}$, then we have $\tau_\ell^\zeta \leq C_\gamma t_\ell^{\zeta-\zeta/\gamma} N^{-\zeta}$ with $\ell = n, n-1$. Thus, it holds that

$$\begin{aligned} t_{n-2}^{\iota-2} (\tau_{n-1} + \tau_n)^2 &\leq C_\gamma \left(t_{n-1}^{\iota-2+\zeta-\zeta/\gamma} \tau_{n-1}^{2-\zeta} N^{-\zeta} + t_n^{\iota-2+\zeta-\zeta/\gamma} \tau_n^{2-\zeta} N^{-\zeta} \right) \\ &= C_\gamma \left(t_{n-1}^{\iota-\zeta/\gamma} (\tau_{n-1}/t_{n-1})^{2-\zeta} N^{-\zeta} + t_n^{\iota-\zeta/\gamma} (\tau_n/t_n)^{2-\zeta} N^{-\zeta} \right) \\ &\leq C_\gamma t_n^{\max\{0, \iota-2/\gamma\}} N^{-\zeta}. \end{aligned}$$

Finally, by inserting the above estimates into (2.16), we complete the proof of (2.17).

Appendix B. Proof of Theorem 4.3

For any $\mathfrak{s} \geq 1$, we assume that $\|\hat{\phi}_{(\mathfrak{s}-1)}^1\|_\infty \leq \beta$, which further implies $\|\hat{\phi}_{(\mathfrak{s}-1)}^{1-\zeta}\|_\infty \leq \beta$. Equivalently, equation (4.8) can be rewritten as

$$((B_0^{(1)} + \kappa(1-\zeta)m)I - (1-\zeta)m\varepsilon^2 \Delta_h) \hat{\phi}_{(\mathfrak{s})}^1 = \mathbf{M}_1 \phi^0 + m(\kappa \hat{\phi}_{(\mathfrak{s}-1)}^{1-\zeta} + f(\hat{\phi}_{(\mathfrak{s}-1)}^{1-\zeta})),$$

where $\mathbf{M}_1 = (B_0^{(1)} - \kappa\zeta m)I + \zeta m \varepsilon^2 \Delta_h$. Due to $B_0^{(1)} \geq \frac{4}{11} \int_{t_0}^{t_1} \frac{\omega_{1-\alpha}(t_1-s)}{\tau_1} ds = \frac{4\tau_1^{-\alpha}}{11\Gamma(2-\alpha)}$ (see Lemma 4.1 (i)), it then follows from (4.9) that all elements of \mathbf{M}_1 are nonnegative, and thus, we have

$$\|\mathbf{M}_1\|_\infty \leq B_0^{(1)} - \kappa\zeta m,$$

which together with Lemmas 2.3–2.4 gives us

$$(B_0^{(1)} + \kappa(1-\zeta)m)\|\hat{\phi}_{(\mathfrak{s})}^1\|_\infty \leq (B_0^{(1)} - \kappa\zeta m)\|\phi^0\|_\infty + \kappa m\beta = (B_0^{(1)} + \kappa(1-\zeta)m)\beta.$$

Consequently, $\|\hat{\phi}_{(\mathfrak{s})}^1\|_\infty \leq \beta$ holds for any $\mathfrak{s} \geq 1$.

Furthermore, (4.8) is also equivalent to

$$\frac{B_0^{(1)}}{1-\zeta}(\hat{\phi}_{(\mathfrak{s})}^{1-\zeta} - \phi^0) = -m(-\varepsilon^2 \Delta_h \hat{\phi}_{(\mathfrak{s})}^{1-\zeta} - f(\hat{\phi}_{(\mathfrak{s}-1)}^{1-\zeta}) + \kappa(\hat{\phi}_{(\mathfrak{s})}^{1-\zeta} - \hat{\phi}_{(\mathfrak{s}-1)}^{1-\zeta})), \quad \mathfrak{s} \geq 1,$$

which defines a mapping $\mathcal{T}[v] = w$ from \mathbb{V}_β to \mathbb{V}_β , i.e.,

$$\frac{B_0^{(1)}}{1-\zeta}(w - \phi^0) = -m(-\varepsilon^2 \Delta_h w - f(v) + \kappa(w - v)), \quad v \in \mathbb{V}_\beta.$$

Similar as in Theorem 2.5, it is straightforward to verify that \mathcal{T} is a contractive mapping under the time-step condition (4.10). Consequently, the iterative scheme (4.8) admits a unique fixed point in \mathbb{V}_β , denoted by $\hat{\phi}^{1-\zeta}$, and $\hat{\phi}^1 = \frac{\phi^{1-\zeta} - \zeta\phi^0}{1-\zeta}$ is just the unique solution of the nonlinear scheme (4.3). The proof of Theorem 4.3 is completed.

References

- [1] M. Ainthworth and Z. Mao. Analysis and approximation of a fractional Cahn–Hilliard equation. *SIAM J. Numer. Anal.*, 55:1689–1718, 2017.
- [2] G. Akagi, G. Schimperna, and A. Segatti. Fractional Cahn–Hilliard, Allen–Cahn and porous medium equations. *J. Differ. Equ.*, 261:2935–2985, 2016.
- [3] A. Alikhanov. A new difference scheme for the time fractional diffusion equation. *J. Comput. Phys.*, 280:424–438, 2015.
- [4] S. Allen and J. Cahn. A microscopic theory for antiphase boundary motion and its application to antiphase domain coarsening. *Acta Metall.*, 27:1085–1095, 1979.
- [5] D. Anderson, G. McFadden, and A. Wheeler. Diffuse-interface methods in fluid mechanics. *Annu. Rev. Fluid Mech.*, 30:139–165, 1998.
- [6] J. Cahn and J. Hilliard. Free energy of a nonuniform system I: Interfacial free energy. *J. Chem. Phys.*, 28:258–267, 1958.
- [7] L. Chen, J. Zhao, W. Cao, H. Wang, and J. Zhang. An accurate and efficient algorithm for the time-fractional molecular beam epitaxy model with slope selection. *Comput. Phys. Commun.*, 245:106842, 2019.

- [8] Q. Du, L. Ju, X. Li, and Z. Qiao. Maximum principle preserving exponential time differencing schemes for the nonlocal Allen–Cahn equation. *SIAM J. Numer. Anal.*, 57:875–898, 2019.
- [9] Q. Du, L. Ju, X. Li, and Z. Qiao. Maximum bound principles for a class of semilinear parabolic equations and exponential time-differencing schemes. *SIAM Rev.*, 63:317–359, 2021.
- [10] Q. Du, C. Liu, and X. Wang. A phase field approach in the numerical study of the elastic bending energy for vesicle membranes. *J. Comput. Phys.*, 198:450–468, 2004.
- [11] Q. Du, J. Yang, and Z. Zhou. Time-fractional Allen–Cahn equations: Analysis and numerical methods. *J. Sci. Comput.*, 85:42, 2020.
- [12] A. Hawkins-Daarud, K. Zee, and J. Oden. Numerical simulation of a thermodynamically consistent four-species tumor growth model. *Int. J. Numer. Methods Biomed. Eng.*, 8:3–24, 2012.
- [13] D. Hou, L. Ju, and Z. Qiao. A linear second-order maximum bound principle-preserving BDF scheme for the Allen–Cahn equation with a general mobility. *Math. Comp.*, 92:2515–2542, 2023.
- [14] D. Hou and C. Xu. Highly efficient and energy dissipative schemes for the time fractional Allen–Cahn equation. *SIAM J. Sci. Comput.*, 43:A3305–A3327, 2021.
- [15] T. Hou, T. Tang, and J. Yang. Numerical analysis of fully discretized Crank–Nicolson scheme for fractional-in-space Allen–Cahn equations. *J. Sci. Comput.*, 72:1–18, 2017.
- [16] Q. Huang, Z. Qiao, and H. Yang. Maximum bound principle and non-negativity preserving ETD schemes for a phase field model of prostate cancer growth with treatment. *Comput. Methods Appl. Mech. Engrg.*, 426:116981, 2024.
- [17] M. Inc, A. Yusuf, A. Aliyu, and D. Baleanu. Time-fractional Cahn–Allen and time-fractional Klein–Gordon equations: lie symmetry analysis, explicit solutions and convergence analysis. *Physica A Stat. Mech. Appl.*, 493:94–106, 2018.
- [18] B. Ji, H. Liao, Y. Gong, and L. Zhang. Adaptive second-order Crank–Nicolson time-stepping schemes for time-fractional molecular beam epitaxial growth models. *SIAM J. Sci. Comput.*, 42:B738–B760, 2020.
- [19] B. Ji, H. Liao, and L. Zhang. Simple maximum principle preserving time-stepping methods for time-fractional Allen–Cahn equation. *Adv. Comput. Math.*, 46:37, 2020.
- [20] B. Jin, R. Lazarov, and Z. Zhou. An analysis of the L1, scheme for the subdiffusion equation with nonsmooth data. *IMA J. Numer. Anal.*, 36:197–221, 2016.
- [21] L. Ju, X. Li, and Z. Qiao. Generalized SAV-exponential integrator schemes for Allen–Cahn type gradient flows. *SIAM J. Numer. Anal.*, 60:1905–1931, 2022.
- [22] L. Ju, X. Li, and Z. Qiao. Stabilized exponential-SAV schemes preserving energy dissipation law and maximum bound principle for the Allen–Cahn type equations. *J. Sci. Comput.*, 92:66, 2022.

- [23] Z. Li, H. Wang, and D. Yang. A space-time fractional phase-field model with tunable sharpness and decay behavior and its efficient numerical simulation. *J. Comput. Phys.*, 347:20–38, 2017.
- [24] H. Liao, D. Li, and J. Zhang. Sharp error estimate of the nonuniform $L1$ formula for linear reaction-subdiffusion equations. *SIAM J. Numer. Anal.*, 56:1112–1133, 2018.
- [25] H. Liao, W. Mclean, and J. Zhang. A second-order scheme with nonuniform time steps for a linear reaction-subdiffusion problem. *Commun. Comput. Phys.*, 30:567–601, 2021.
- [26] H. Liao, T. Tang, and T. Zhou. A second-order and nonuniform time-stepping maximum-principle preserving scheme for time-fractional Allen–Cahn equations. *J. Comput. Phys.*, 414:109473, 2020.
- [27] H. Liao, T. Tang, and T. Zhou. An energy stable and maximum bound preserving scheme with variable time steps for time fractional Allen–Cahn equation. *SIAM J. Sci. Comput.*, 43:A3503–A3526, 2021.
- [28] H. Liao, T. Tang, and T. Zhou. Positive definiteness of real quadratic forms resulting from the variable-step $L1$ -type approximations of convolution operators. *Sci. China Math.*, 67:237–252, 2024.
- [29] H. Liao, X. Zhu, and H. Sun. Asymptotically compatible energy and dissipation law of the nonuniform $L2-1_\sigma$ scheme for time fractional Allen–Cahn model. *J. Sci. Comput.*, 99:46, 2024.
- [30] Y. Lin and C. Xu. Finite difference/spectral approximations for the time-fractional diffusion equation. *J. Comput. Phys.*, 225:1533–1552, 2007.
- [31] H. Liu, A. Cheng, H. Wang, and J. Zhao. Time-fractional Allen–Cahn and Cahn–Hilliard phase-field models and their numerical investigation. *Comput. Math. Appl.*, 76:1876–1892, 2019.
- [32] K. Mustapha, B. Abdallah, and K. Furati. A discontinuous Petrov–Galerkin method for time-fractional diffusion equations. *SIAM J. Numer. Anal.*, 52:2512–2529, 2014.
- [33] R. Qi and X. Zhao. A unified design of energy stable schemes with variable steps for fractional gradient flows and nonlinear integro-differential equations. *SIAM J. Sci. Comput.*, 46:A130–A155, 2024.
- [34] T. Qian, X. Wang, and P. Sheng. Molecular scale contact line hydrodynamics of immiscible flows. *Phys. Rev. E*, 68:016306, 2003.
- [35] Z. Qiao, Z. Zhang, and T. Tang. An adaptive time-stepping strategy for the molecular beam epitaxy models. *SIAM J. Sci. Comput.*, 33:1395–1414, 2011.
- [36] C. Quan and B. Wang. Energy stable $L2$ schemes for time-fractional phase-field equations. *J. Comput. Phys.*, 458:111085, 2022.
- [37] J. Shen and J. Xu. Convergence and error analysis for the scalar auxiliary variable (SAV) schemes to gradient flows. *SIAM J. Numer. Anal.*, 56:2895–2912, 2018.

- [38] J. Shen, J. Xu, and J. Yang. The scalar auxiliary variable (SAV) approach for gradient flows. *J. Comput. Phys.*, 353:407–416, 2018.
- [39] M. Stynes, E. O’Riordan, and J. Gracia. Error analysis of a finite difference method on graded meshes for a time-fractional diffusion equation. *SIAM J. Numer. Anal.*, 55:1057–1079, 2017.
- [40] Z. Sun and X. Wu. A fully discrete difference scheme for a diffusion-wave system. *Appl. Numer. Math.*, 56:193–209, 2006.
- [41] T. Tang and J. Yang. Implicit-explicit scheme for the Allen–Cahn equation preserves the maximum principle. *J. Comput. Math.*, 34:471–481, 2016.
- [42] T. Tang, H. Yu, and T. Zhou. On energy dissipation theory and numerical stability for time-fractional phase-field equations. *SIAM J. Sci. Comput.*, 41:A3757–A3778, 2019.
- [43] S. Wise, J. Lowengrub, H. Frieboes, and V. Cristini. Three-dimensional multispecies nonlinear tumor growth I: Model and numerical method. *J. Theor. Biol.*, 253:524–543, 2008.
- [44] C. Xu and T. Tang. Stability analysis of large time-stepping methods for epitaxial growth models. *SIAM J. Numer. Anal.*, 44:1759–1779, 2006.
- [45] G. Zhang, C. Huang, A. Alikhanov, and B. Yin. A high-order discrete energy decay and maximum-principle preserving scheme for time fractional Allen–Cahn equation. *J. Sci. Comput.*, 96:39, 2023.
- [46] Z. Zhang and Z. Qiao. An adaptive time-stepping strategy for the Cahn–Hilliard equation. *Commun. Comput. Phys.*, 11:1261–1278, 2012.